Experimental dataset for an AHU air-to-air heat exchanger with normal and simulated fault operations

Hugo Geoffroy, Julien Berger, Evelyne Gonze, Catherine Buhe

Experimental dataset for an AHU air-to-air heat exchanger with normal and simulated fault operations

Hugo Geoffroy[a], Julien Berger [b*], Evelyne Gonze [a], Catherine Buhe[a]

November 8, 2022

[a] Univ. Grenoble Alpes, Univ. Savoie Mont Blanc, CNRS, LOCIE, 73000 Chambéry, France
[b] Laboratoire des Sciences de l'Ingénieur pour l'Environnement (LaSIE), UMR 7356 CNRS, La Rochelle Université, CNRS, 17000, La Rochelle, France
[*] corresponding author: julien.berger@univ-lr.fr

Abstract

Fault Detection and Diagnosis (FDD) is an important tool in building commissioning. Providing a consolidated dataset for FDD benchmarking is necessary to accurately evaluate the FDD prediction accuracy and detect anomalies. In this study, we provide an experimental dataset for an air handling unit containing two ducts linked by an air-to-air heat exchanger. The dataset is composed of nominal and faulty operations of the system, including the ground truth in order to investigate various faults in 52 cases. The dataset was obtained by measuring a representative system with real climate variations like the ones obtained by Building Automation Systems. The transition between nominal and fault sequences was continuous, as in real operating conditions. An uncertainty evaluation was carried out to provide confidence bounds in the experimental dataset.

Key words: Fault detection and diagnosis; experimental dataset; air handling unit; benchmarking ; Heating Ventilation and Air-Conditioning systems

1 Introduction

According to the United States Department of Energy, the building sector is the biggest consumer of primary energy in the USA, with 41 % of the total energy consumption [1]. Of this huge energy use, 50 % is directly consumed by Heating, Ventilation and Air-Conditioning (HVAC) systems [2]. It is also known that HVAC systems usually do not function as required, causing additional and unnecessary energy consumption: a recent study showed that HVAC operation problems can result in waste between 25 % and 50 % of energy loss [3]. These HVAC operation problems may derive from different factors such as failed sensory devices or actuators, inappropriate setpoints and schedules or controller programming errors. For these reasons, the commissioning of HVAC systems in existing buildings is a major issue.

The aim of building commissioning is to resolve this issue with monitored data obtained through Building Automation Systems (BAS). In particular, simple and automated Fault Detection and Diagnosis (FDD) tools have been developed to assist the work-orders in commissioning. With good commissioning, energy consumption can be reduced by 15% . Nowadays, the required characteristics of FDD for HVAC systems are known. Venkatasubramanian listed ten criteria: quick detection and diagnosis, isolability, robustness, novelty identifiability, classification error estimate, adaptability, explanation facility, modelling requirement and multiple fault identifiability [4]. All these characteristics need to be evaluated and compared for various FDD tools.

Several studies have been carried out to propose metrics for FDD evaluation [5, 6]. A procedure for performance evaluation has been proposed [5] and recently improved in [7, 8]. In [9], an updated review of FDD tools was proposed that separates the different tasks with a thorough comparison. In [9], the authors suggested some perspectives for the improvement for FDD. Benchmarking FDD performance in particular

requires a standard data set for testing procedures. Previous studies used numerical deterministic data generated with models [10–12]. Although case studies in real buildings can be found in the literature [13–15], according to [16, 17], only two standard public experimental datasets are available for FDD evaluation through the ASHRAE RP 1020 and 1312 [18, 19]. In the above-mentioned studies, the following observation was often made: there is a lack of standard input data that would allow an "apple to apple" comparison. In other words, datasets should have an appropriate balance between the number of faulty and non-faulty observations to avoid introducing bias into the FDD evaluation. Thus, providing a consolidated dataset for FDD benchmarking is important. This may be a first step toward reducing the gap between research and the real challenges people face in the field [20].

Within this context, the aim of this paper is to propose a specific experimental dataset for an Air Handling Unit (AHU) with supply and exhaust ducts. A heat exchanger links both ducts to heat the outside air in winter. Note that the method can be applied to other types of HVAC systems. The choice of this system was made for several reasons. First, mechanical ventilation systems are widely used to provide clean air to the building occupants. Secondly, the increasing energy efficiency regulations, systems for energy recuperation from the exhaust air have become very common for residential and commercial buildings [21, 22]. Thirdly, with the increase in indoor air quality concerns, the commissioning of such a system may become crucial. Indeed, building energy efficiency and indoor air quality requirements are difficult to reconcile. finally, a significant number of studies have been carried out on FDD tools applied to AHU systems [23–27].

The originality of the our dataset is based on several points. These results could be used by researchers for developing benchmarking models of FDD, and testing some new developments of FDDs. It is composed of various nominal and AHU faulty operations for both winter and summer configurations. Several hard, soft and operation faults were investigated. Note that these investigations focused on the above-described AHU itself and not on zone-level equipment or sensor anomalies. The dataset is representative of real building cases recorded using BAS with similar sensors including the background noise like field data. Attention was payed to the ground truth of the faulty cases [28, 29]. For this, a complete uncertainty propagation of the experimental data was performed. Moreover, to have a consensus statement, the faulty operation dataset was compared to a nominal one. The occurrence of the faults was almost continuous due to high frequency monitoring. This enabled us to observe carefully the transition between a normal and a faulty operation. Finally, these experimental data represent real phenomena, richer than simulated measurements that include model error and bias.

This article is organized as follows. In Section 2, the experimental design and the AHU system to generate the experimental dataset are described. A precise description of the monitoring system is also given. Then, in Section 3, the dataset is presented. Finally, Section 4 gives some concluding remarks and guidelines for future work.

2 Methodology

This section presents the methodology, the experimental design and the system used to generate the experimental dataset.

2.1 General overview

Figure 1 gives an overview of the methodology. An AHU unit with an air-to-air heat exchanger was used for the investigations. The equipment was monitored with BAS sensors. Two experimental data sets were then generated for both nominal and faulty operations.

The AHU corresponds to a system that can be found in residential and medium commercial buildings and is presented in Figure 2. It works with a constant air volume using a single duct system with a maximal airflow of 260 $m^3.h^{-1}$. It supplies fresh air for up to seven different rooms, in conformity with the French regulations [30]. The AHU is composed of a supply duct, which processes the outside air before insufflation, and an exhaust duct which collects the inside air and expels it outdoors. The supply duct includes fresh and blown air ducts, and the exhaust duct, the return duct and a exoelled air ducts. Furthermore, an air to

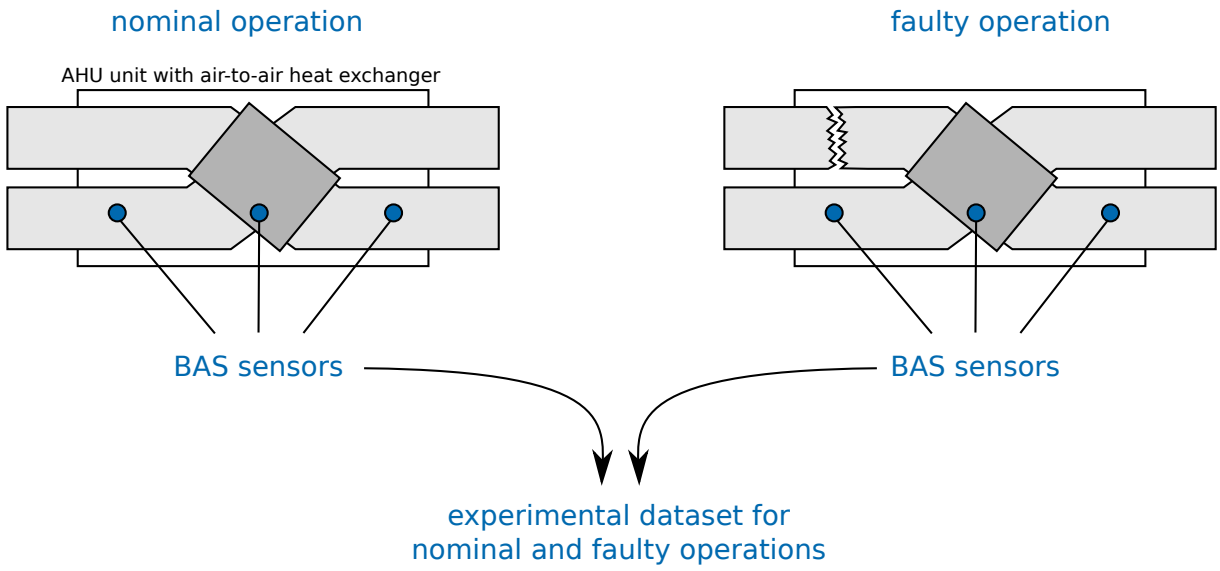

Figure 1. *Illustration of the methodology.*

air heat exchanger completes the equipment so the outside air is warmed before being injected. The plate type exchanger works in counter flow with a bypass damper. An electric coil was positioned upstream to the exchanger to avoid any freezing on the plate. Downstream to the exchanger, another electric coil was installed for additional heating of the air to reach a defined set-point. Four air dampers were set to adjust the airflows. Two were located in the supply duct on the fresh air and blown air ducts, respectively. Two more dampers were placed in the exhaust air duct on the return and the rejected air ducts, respectively. The ducts were protected from the environment by inlet and outlet protections.

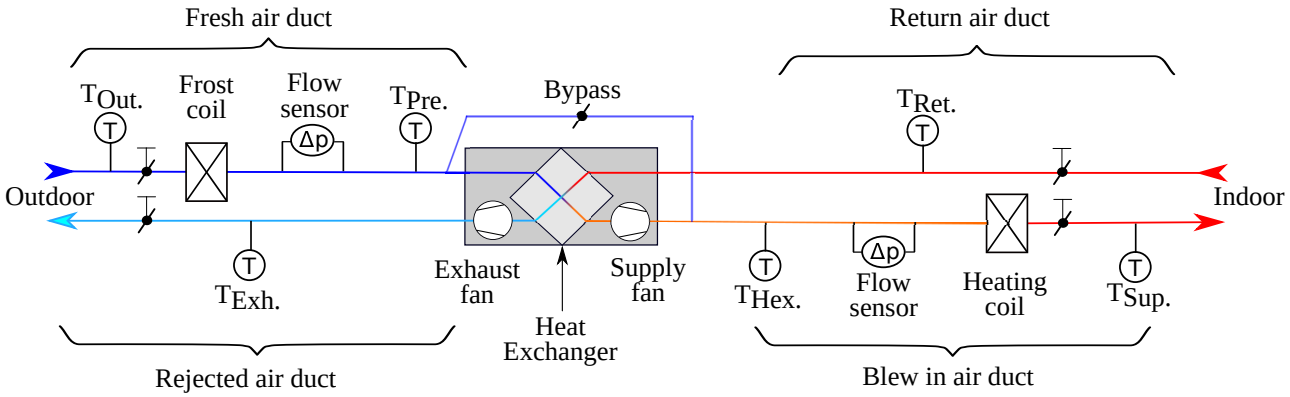

Figure 2. *Schematic representation of the system.*

The test room is illustrated in Figure 3. It is situated on the first floor of a school building and has two outside walls, oriented 250° West and 160° South. The South facade has an outside door (1.9 m × 2.1 m). The West wall has four windows out of a total of 12 m^2 (three times 2.6 m × 3.3 m and one of 2.3 m × 1.48 m). There are two other inside doors. The surface of the room is 84 m^2 and the ceiling is 2.64 m. It has roughly the configuration of a three room apartment.

Regarding the French regulations [30], a four room house must have an airflow of at least 90 $m^3.h^{-1}$. This increases to 120 $m^3.h^{-1}$ when there is a specific generation of internal pollution such as cooking. This is equivalent to an air exchange rate between 0.4 $vol.h^{-1}$ and 0.55$vol.h^{-1}$. Similar values can be obtained for a complex of five individual offices using the corresponding French regulations [31]. Thus, it is a consistent hypothesis regarding the surface area of the room.

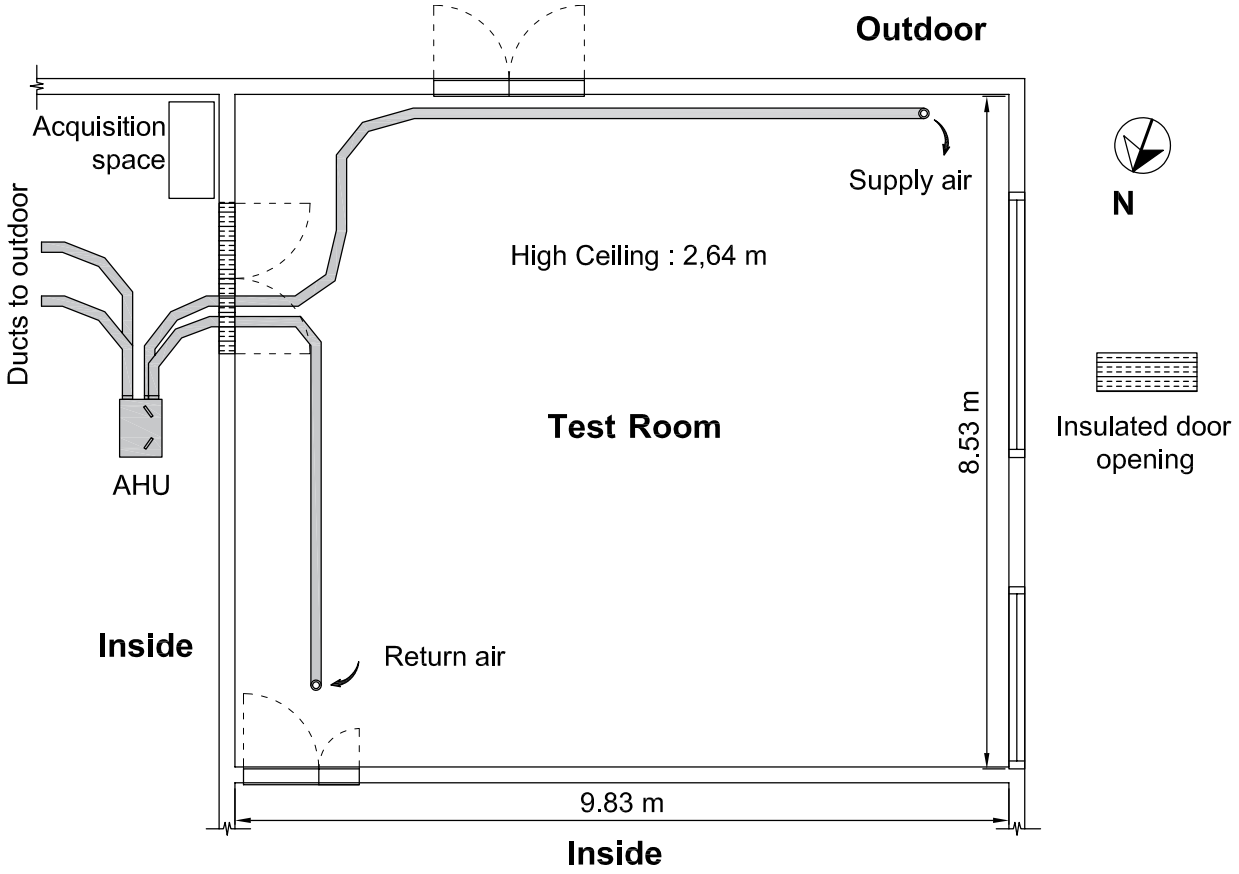

Figure 3. *Schematic representation of the test room with the AHU system.*

As represented in Figure 3 the AHU is located in an uncontrolled room next to the test room. It is representative of the case where the AHU is stored in a technical room. This may be different to the case where the system is placed on a roof. The change in temperature in the ducts may be different, particularly when there is an airflow problem (stagnant air). For this reason, the ducts were insulated to reduce as much as possible the difference between these two cases.

2.2 Equipment details

Most of the constant air volume system emanates from the same product line. The DFX 90 air handling unit of the *France Air* supplier, shown in the Figure 4, was used as the basic system in our study. It is composed of two fans, two filters, an air recovery system and an associated bypass. The DFX 90 was improved by two heating coils and manual and circular dampers.

The heat exchanger structure has 25 mm of polystyrene insulation protected by a galvanised steel shell. The two low-pressure axial fans are are powered by a single-phase supply of 230 V at 50 Hz. A switch allows the selection of high or low fan speed.

The filters on the supply air and the exhaust air are ISO ePM10 50% (M5) and ISO coarse 90% (G4), respectively. The nominal efficiency of the heat exchanger is 90% according to the constructor data-sheet. The bypass of the heat recovery system has only two positions, fully opened or closed. The supply air inlet in the constant air volume system (from the fresh air duct) and the supply air outlet (to the blow-in air branch) flow through a 125 mm diameter connection. Regarding the expelled air, the air from the return air duct enters the AHU through a 125 mm and four 80 mm diameter connections, and the air to the rejected air duct leaves through a 125 mm diameter connection. The unused return air openings can be closed with covers. The return and blow-in air duct are insulated.

The two electric coils (defrost and reheat) were also built by *France Air* company, referenced as SYSTAIR

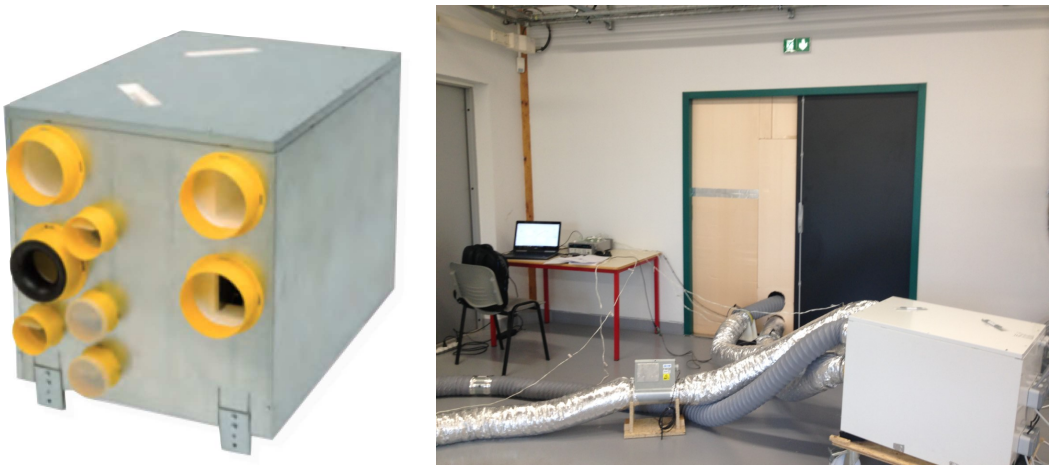

(a) (b)

Figure 4. *DFX*90 *Dual flow AHU from* France Air.

CIREC A 2. They were powered by mono-phased electricty of 230 V at 50 Hz, which provides a maximal power of 1.6 kW. They must operate with a minimal flow of 95 $m^3.h^{-1}$. They were controlled with respect to temperature ranges, so two temperature values had to be set in the PID controller.

The circular dampers were controlled manually acting on the flow rate by pressure loss. They were placed on the four main ducts as reported in Figure 4, and an airflow balance between the ducts. They are made of 125 mm diameter galvanised steel from *CAIROX*, with class C airtightness, based on the European regulation EN 1751.

2.3 Monitoring procedure

2.3.1 Data

Regarding the sensors on the AHU, there were three kinds of monitored information: *(i)* the temperature of the air; *(ii)* the pressure drop on the diaphragms; and *(iii)* the electricity consumed by the electrical equipment. These data were recorded together with the usual information in BAS, which are temperature, airflow, the state of the control equipment and the power of the equipment [32–36]. The temperatures selected for the study are representative of indoor and outdoor conditions, and the temperatures used to evaluate the performance of an air-to-air exchanger and the operation of the heating coils. The two airflows were recorded to check the airflow balance since they are also used in the evaluation of the exchanger performance. The power consumption of all the electrical components was also measured for control purposes. All the measurements were projected in real-time during the tests on a *Labview* interface to verify the monitoring procedure of the experiments.

The air temperatures $T\ [\ ^\circ C\ ]$ were recorded at six points in the ducts. Four temperatures were monitored in the supply duct on the fresh and blow-in air ducts, respectively. For the primer, the temperature was monitored at the system supply duct air inlet, corresponding to the outdoor air T_{out} and before the heat exchanger T_{pre}, standing for the pre-heated air. For the latter, the temperature was recorded after the heat exchanger T_{hex}, and after the heating coil corresponding to the supply air T_{sup}. Two additional measurements were made in the exhaust duct, the return and reject air duct. For the return air duct, the temperature was recorded at the inlet of the pipe,and is the return air temperature T_{ret} corresponding to the interior room temperature. Regarding the expelled air branch, the sensor is located after the heat exchanger related to the exhaust air temperature T_{exh}. The location of these temperature sensors is shown in Figure 2. It is important to note that all temperatures were measured under physical redundancy by two thermocouples. Then, the mean temperature for each point was calculated and used for the investigation. This redundancy enables to increased the accuracy of the experimental dataset.

In this study, heating coils were not used. Therefore, the temperature of the pre-heat air, after the defrost heating coil, was assumed to be equal to the outside temperature $T_{pre} \approx T_{out}$. The same hypothesis is valid for the temperature at the heat exchanger outlet and the supply air temperature $T_{hex} \approx T_{sup}$. This hypothesis was verified for each dataset by certifying that the standard deviation between the two fields is lower than the maximal measurement uncertainty (of around 0.3 $°C$).

All temperatures were measured using thermocouple sensor technology. Two types of thermocouples were used according to the European EN 60 584 regulation a nickel-chrome/nickel known as K-type, and a copper/copper-nickel known as T-type. The measurements were gathered directly using a switch unit *KEYSIGHT 34972A LXI Data Acquisition* with a five seconds time step. The recording time step was selected to assess precisely the temperature evolution in the system. The choice was made using a rough computation with the minimal air speed in the duct (2.7 $m.s^{-1}$) and the maximal distance of the temperature sensors in the same duct (around 10 m). Thus, a five second time step was selected for each sensor so that the transient behaviour of the system could be recorded with accuracy. Note that this acquisition frequency is more precise than the one used by common BAS (generally of the order of one minute). This short time step can be easily processed to obtain a coarser time step.

During the preliminary phase, all the thermocouples were calibrated by comparison to a reference sensor, which was a four wired PT100 called AN5847 from AOIP. The calibration was performed in the range $[-20, 45]$ $°C$ with a discretization every 5 $°C$ (16 steps), during a phase of increasing temperature. The calibration procedure is the following: all the thermocouples and the reference sensor were immersed in a temperature-controlled glycol bath, and all the sensors were also placed in a copper block to homogenise the bath temperature. Sixteen temperature steps were carried out. Each one lasted ten minutes. The temperature was recorded with a five second time step and the mean temperature for each sensor was used for the calibration. A third-order correction polynomial was then computed to minimise the error of each sensor regarding the reference. Then, a verification phase was carried out for every temperature in the range $[-20, 45]$ $°C$ with a discretization every 5 $°C$, during a decreasing temperature phase. The correlation coefficient was determined for all the thermocouples after correction. The value of each coefficient was between 0.99 and 1 with a maximal standard deviation on all the calibration ranges of 0.2092 $°C$.

As mentioned before, circular dampers were used to control the airflow. Thus, airflow could be measured by pressure differences Δp $[Pa]$ on each side of the damper using diaphragm technology sensors. The pressure sensors were the SDP610 Series obtained from the *Sensirion* company. According to the constructor data-sheet, the span accuracy is 3% of the reading measurement. The *Sensirion* sensors were connected to an *Arduino* UNO micro-controller for data recording. As for the temperature, a five second time step was chosen for the measurements.

Finally, all the power P $[W]$ consumed by the electrical devices was measured using the *Energy Logger 4000* device from *Voltcraft*. According to the supplier the accuracy of the meter varies between 1% and 15% depending on the measuring ranges. The data were collected using a logger on a Secure Digital card with a 60 second time step. Such logger cannot record the power with a lower time step. Thus, power data are recorded with a coarser time step compared to other data (5 seconds for temperature and airflow). Table 1 provides a summary of the uncertainty of the measured fields.

2.3.2 Computed data

Using the previously described measurements, three important quantities were computed. First, since the direct measurement of an aeraulic airflow is difficult and very uncertain, we preferred to measure a pressure difference and then compute the corresponding airflow. This is a common method to obtain airflows of aeraulic systems in BAS. That is why the airflow Q_v $[m^3.h^{-1}]$ was computed according to the following equation:

$$Q_v = k \cdot \left(\Delta p\right)^n, \tag{1}$$

where, according to the supplier, $n = 0.5$ and the coefficient k is adjusted depending on the position of the circular damper, varying from 1 to 7 for a given piece of equipment. Then, the total heat exchanger

effectiveness η $[-]$ is given by [37, 38]:

$$\eta = \frac{(T_{sup} - T_{pre}) \cdot Q_{v,sup} \cdot \rho_{sup} \cdot c_{sup}}{(T_{ret} - T_{pre}) \cdot Q_{v,\min} \cdot \rho_{\min} \cdot c_{\min}}, \tag{2}$$

where T_{sup}, T_{pre} and T_{ret} are the post heat exchanger, the pre heat exchanger and the return air duct temperatures, respectively. The quantities ρ $[\mathsf{kg.m^{-3}}]$ and c $[\mathsf{J.kg^{-1}.K^{-1}}]$ are the density and the heat capacity for air, respectively. Both are considered as constant in relation to the temperature range of the study. The quantities with the subscript min are defined as follows:

$$\rho_{\min} = \min(\rho_{sup}, \rho_{exh}), \quad c_{\min} = \min(c_{sup}, c_{exh}), \quad Q_{v,\min} = \min(Q_{v,sup}, Q_{v,exh}), \tag{3}$$

where the subscript *sup* and *exh* stands for the supply and exhaust air ducts, respectively. The third quantity is the heat flux in the heat exchanger ϕ $[\mathsf{W}]$:

$$\phi = Q_{v,\min} \cdot \rho_{pre} \cdot C_{pre} \cdot (T_{hex} - T_{pre}). \tag{4}$$

The subscript *pre* denotes the pre heat exchanger. During the summer, the heat exchanger of the AHU is not used thanks to the bypass. This avoids heating the building for nothing. Thus, Equation (4) was only evaluated in winter. It should be noted that these computed data were used as indicators to check for the appearance of faults and validate the dataset as a ground truth.

2.4 Uncertainty propagation

To consolidate the experimental dataset provided in this work, an error propagation calculation was carried for each important field. Thus, all the results and Figures presented are represented with a grey band highlighting the uncertainty associated with the values. The work and the hypothesis is used to compute the uncertainties are presented below, following the guidelines [39].

To evaluate the uncertainties associated with any given experimental value, three different methods were used. Table 1 provides an overview of the evaluation of uncertainty for each quantity. First, regarding the measurement obtained by physical redundancy (only for the temperature), it is considered that the systematic errors are reduced since the sensors have been calibrated with a certified reference. Thus, the value retained corresponds to the mean of the two measured values. The uncertainty was calculated using the standard deviation of the population, neglecting other bias and errors that may occur.

Regarding the directly measured physical parameter, the uncertainty considered was that of the sensors and given by the manufacturer. Thus, the energy consumption measurement accuracy is 1% from 5 W to 3500 W, 5% from 2 W to 5 W and 15% for values under 2 W, according to Voltcraft. The pressure value was also directly measured by the sensor with a precision of 3%. For these two physical values, the represented uncertainty is evaluated as the accuracy of the sensors. Note that other sources of random errors might exist but assumed as negligible here.

Finally, for the computed physical values (airflow, the efficiency and heat exchanger gain), the uncertainty propagation was calculated using the method proposed in [40, 41]. The general formula of uncertainty of the quantity f is the following:

$$\sigma_f = \sqrt{\sum_{i=1}^{N} \left(\frac{\partial f}{\partial x_i} \cdot \sigma_{x_i} \right)^2}, \tag{5}$$

where x_i is one of the N uncertain variables of f and σ_{x_i} is the standard deviation of x_i. Note that the random error of the measurement cannot be evaluated. Indeed, experiments were carried out with a real case study in which the system was exposed to varying outside climatic conditions. Thus, it is impossible to repeat the experiments with the exact same outside conditions to evaluate such error. As suggested in [39], a probability that the true value lies within the stated range should be evaluated and mentioned by the experimenter. Here, the probability was evaluated as 95 % for all quantities.

Thus, the uncertainty of the airflow is given using Eq. (1). Two uncertain variables were considered: the damper coefficient k and the pressure difference ΔP, so we have

$$\sigma_Q = \sqrt{\left(\frac{\partial Q_v}{\partial k}\cdot\sigma_k\right)^2 + \left(\frac{\partial Q_v}{\partial p}\cdot\sigma_p\right)^2} \tag{6}$$

where σ_k and σ_p are the damper coefficient and pressure difference uncertainties. The quantities $\frac{\partial Q_v}{\partial k}$ and $\frac{\partial Q_v}{\partial p}$ were obtained by direct differentiation of Eq. (1). The value of the uncertainty depends on the pressure difference Δp as well as the coefficients n and k. Considering the minimum pressure difference given by the measurement uncertainty $\Delta p = 0.1\ \mathsf{Pa}$ and the coefficient $k = 7$, one obtains the minimum accuracy of the airflow $\sigma_Q = = 5\cdot 10^{-7}\ \mathsf{m^3.h^{-1}}$, which is approximated to $\sigma_Q \approx 0$ in Table 1.

Regarding Eq. (2) for heat efficiency, uncertainty is given by:

$$\sigma_\eta = \sqrt{\left(\frac{\partial \eta}{\partial Q_v}\cdot\sigma_Q\right)^2 + \left(\frac{\partial \eta}{\partial T}\cdot\sigma_T^{\max}\right)^2}, \tag{7}$$

where σ_Q is the airflow uncertainty given by Eq. (6) and $\sigma_T^{\max}$ is the temperature related uncertainty. This corresponds to two-times the maximal uncertainty of the sensors, evaluated during the pre-calibration phase. Given the values of Table 1, we have $\sigma_T^{\max} = 2\cdot 0.062\ \mathsf{K}$. The quantities $\frac{\partial \eta}{\partial Q_v}$ and $\frac{\partial \eta}{\partial T}$ were obtained by direct differentiation of Eq. (2). Finally, the heat flux uncertainty is:

$$\sigma_\phi = \sqrt{\left(\frac{\partial \phi}{\partial Q_v}\cdot\sigma_Q\right)^2 + \left(\frac{\partial \phi}{\partial \rho}\cdot\sigma_\rho\right)^2 + \left(\frac{\partial \phi}{\partial C}\cdot\sigma_C\right)^2 + \left(\frac{\partial \phi}{\partial T}\cdot\sigma_T^{\max}\right)^2} \tag{8}$$

where σ_ρ and σ_C are the pre-heat air density and heat capacity uncertainties, respectively. The partial derivatives were obtained from direct differentiation of Eq. (4).

Table 1. *Summary of the measured quantities and their uncertainties.*

Quantity	**Uncertainty evaluation**	**Values**
Temperature T	physical redundancy	$\sigma_T \in \left[6.36\cdot 10^{-6}, 0.062\right]\ \mathsf{K}$
Air flow Q_v	propagation of uncertain variables k and p	$\sigma_k = 3.6$
		$\sigma_p = 0.1\ \mathsf{Pa}$
		$\sigma_Q \in \left[0, 24.84\right]\ \mathsf{m^3.h^{-1}}$
Heat exchanger efficiency η	propagation of uncertain variables T and Q_v	$\sigma_T \in \left[0.018, 0.298\right]\ \mathsf{K}$
		$\sigma_Q \in \left[0, 24.84\right]\ \mathsf{m^3.h^{-1}}$
Exchanged heat flux ϕ	propagation of uncertain variables	$\sigma_Q \in \left[0, 24.84\right]\ \mathsf{m^3.h^{-1}}$
	Q_v, ρ_{pre}, C_{pre} and T	$\sigma_\rho \in \left[0.0237, 0.0241\right]\ \mathsf{kg.m^{-3}}$
		$\sigma_C = 1.5075\ \mathsf{J.kg^{-1}.K^{-1}}$
		$\sigma_T \in \left[0.032, 0.298\right]\ \mathsf{K}$

It is important to underline the importance of uncertainty in the measured dataset. The analysis of uncertainty is significant and is used to validate the appearance of faulty behavior. It can be verified that the fault is not included in the uncertainty of the measurement. So uncertainty takes an important part of the ground truth.

2.5 Generation of a dataset for nominal and faulty system operation

The aim of this study was to generate an experimental dataset using the system described above. A dataset was produced for both nominal and faulty operations. This paper only presents the data generated during both summer and winter seasons. All the tests were performed between mid June and mid October 2019 for the summer season, and between December 2019 and February 2020 for the winter. The climate recorded during the dataset generation is presented in Figure 5 for both campaigns.

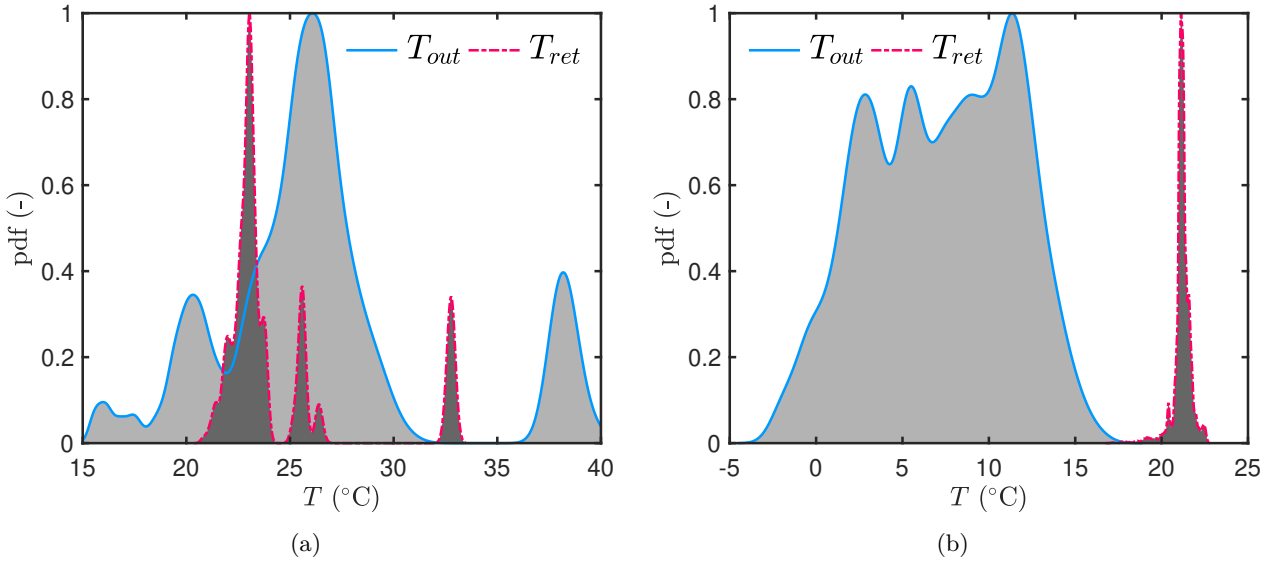

Figure 5. *Probability density function of the temperature during the summer* (a) *and winter* (b) *campaigns.*

2.5.1 Fault definition

First, it is important to define what is considered as a fault in this study. We considered faults to be any state or behavior that prevents the system from operating properly. Three main categories of faults can be distinguished: *(i)* a hard fault, *(ii)* a soft fault [10, 42, 43] and *(iii)* a control fault. A hard fault occurs suddenly and involves a complete failure of the system. Examples are a breakdown of a pump, a fan belt break or actuator failure.

Soft faults are those that shift the system from the optimal or designed performance. They do not induce a complete failure and generally occur gradually over a period of time. They are common and are more complex to detect due to their progressive apparition. Moreover, the impact on the system efficiency is low and a threshold should be chosen to distinguish the difference between a normal and soft degradation. Detection allows the intervention of the maintenance staff to avoid any probable hard faults as well as sanitary or comfort issues.

Finally, the so-called operational faults are due to problems with the optimal functional analysis of the system. In other words, the management of the system is not well designed or set up. These faults can be distinguished from soft ones since they are not a consequence of the system in operation, due to a problem with the engineers' configuration. Examples of soft faults can be found in [14, 16, 44, 45], which highlight the importance of investigating them.

The failures can be classified in three classes depending on the season of whih they occur. Faults due to heating components are classified as *winter season faults*. Failure during cooling phases are classified as *summer season faults*. Finally, those which can occur at any time are referred to as *global faults*.

2.5.2 Fault selection

For the sake of compactness, a part of the experimental dataset in the winter and summer configurations is presented in Results Section 3. The failures investigated were those which are usually encountered in air handling units, for the three categories mentioned previously. For hard faults, the selected ones were: a failure of each fan, a fan belt break of each fan and a bypass air damper failure. Concerning the faults, fouling of the air filter and the obstruction of a duct were investigated. Finally, the dataset for operation failure corresponds to control problems of the bypass and free cooling. All the system failures generated in this study are summarized in Table 2. There is a total of 52 cases numbered according to the fourth (right) column of Table 2 (6 for fan failure + 8 for bypass damper failure + 18 for filter fooling + 8 for duct obstruction + 4 for fan belt breakdown + 2 for bypass obstruction + 2 for heat coil failure + 2 for heat coil regulation + 2 for defrost coil failure).

Note that the defrost coil anomaly can be considered a soft fault since it slowly deteriorated with time. Inversely, a sudden break of the defrost coil (due to electrical dysfunction for instance) can be seen as a hard fault. In these investigations, the defrost coil hard fault was provoked suddenly, as a hard fault.

Table 2. *Summary of the faults investigated for the generation of the experimental dataset.*

Fault Name	**Fault type**	**Category**	**Cases generated**
Fan failure	Hard	Global	2 Nominal and 4 faults as a function of fan and speed
Bypass damper failure	Operation	Summer	2 Nominal and 6 faults as a function of fan and speed
Filter fooling	Soft	Global	2 Nominal and 16 faults as a function of fan and speed
Duct obstruction	Soft	Global	8 Faults as a function of speed
Fan Belt Breakdown	Hard	Global	4 Faults as a function of fan and speed
Bypass damper obstruction	Soft	Summer	2 Faults as a function of speed
Heat coil failure	Hard	Winter	2 Faults as a function of speed
Heat coil regulation	Soft	Winter	2 Faults as a function of speed
Defrost coil failure	Hard	Winter	2 Faults as a function of speed

2.5.3 Experimental design for dataset generation

Two types of dataset were generated for each failure. The first corresponds to a nominal process and the second to the system behaviour during a faulty operation. In this way, the anomaly can be better highlighted. All the tests were recorded over at least five minutes, to reach steady state. The experimental design for each dataset will be explained below.

For the nominal fan, the system operates normally. The fans functioned in a steady state, they were suitably powered and supplied a well-balanced airflow. A unique dataset is provided for the nominal operation of the fans for each airflow. For fan failure, the dataset was generated for each ventilator for the two airflow levels. Fan breakdown was achieved using a commutator placed on the fan power cable. During a proper operation of the system, the fan was intentionally "broken" by turning the switch off. Thus, the commutator induced a power failure in the equipment, representing fan failure.

For the fan belt breakdown, this fault was also generated for the two fans and for each airflow level. To generate a belt breakdown, the power was stopped by the commutator. Thus, the airflow decreased until it reached a total standstill in the duct. There was no airflow through the duct recorded by the sensors and the temperature was no longer controlled. But during a belt breakdown fault, the motor is still operating and so

there is still energy consumption. To simulate this behaviour, the fan power data after the shutdown were replaced with data of this same fan operating normally. Thus, the fan belt breakdown data are composed of temperature, pressure loss and airflow data induced by the failure of a fan and power consumption generated by the fan.

The usual bypass operation occurs when building free cooling is required. The bypass is used to stop heat exchange between the outside and return air. To intensify cooling, the airflow is generally increased. Two usual bypass operations were identified for this study. The first is when the system supplies a low airflow which increases when the bypass is activated. The second is when the highest airflow is already provided and the bypass is activated without a modification of the airflow. In both cases, the bypass is activated manually by a commutator when the free-cooling condition occurs. The control sequence of the bypass activation is presented in Eq. 9.

$$Byp_{ON} \stackrel{\text{def}}{:=} T_{ret} - T_{set} \geq 0 \wedge T_{ret} - T_{out} \geq 0\,, \tag{9}$$

where Byp_{ON} is the bypass damper activation, T_{ret} is the room temperature, T_{set} is the set-point (set to 23 °C). To generate the dataset for the bypass damper failure, the airflow commutator and bypass switch were used manually. The faults were generated by activation of the bypass and by modifying the airflow.

The faults for the bypass damper obstruction correspond to a failure of the bypass due to mechanical and not control problems. When the bypass damper is activated, it receives an electrical impulsion to switch on but it cannot because it is blocked. To simulate the obstruction of the bypass, the damper were hampered using an extruded polystyrene block and duct tape. So power is sent to the commutator to move the damper position, but the equipment can not operate properly. To generate these fault data, the temperature and airflow measurements are used from the bypass damper faults were used while the power was measured when the damper was obstructed.

For filter fouling, the same design as nominal fan operation was used to generate the nominal operation dataset with clean filters. For the faults, the aim was to represent situations where dust clogs the filter in the air ducts. In the experimental design, the obstruction was performed from 0% to 80% of the total surface of the filter with steps of 10% . The obstruction of the filter surface was performed using aluminium adhesive tape. Clogging of the filter was achieved with bands as homogeneous as possible placed on the section.

A duct obstruction fault is a hard fault that appears when a careless user of a room seals an air inlet. It can also occur when the system has not been installed carefully and part of the duct is mechanically compressed. This fault can affect the four air ducts. So, each fault was generated by closing the manual damper of the corresponding duct to increase significantly the pressure loss. The three other dampers remained fully open.

The heat and defrost coil faults were generated at two fan speeds. Like hard faults, they occur suddenly after a nominal operation of the system. For heat coil failure, the fault was generated by cutting off the power supply. Thus, the heat coil does not operate when it is needed by the system. Concerning defrost coil regulation failure, this happens due to a PID regulation problem. The controller does not regulate accurately the coil according to the set-up temperature. To generate such a failure, the set-up temperature of the coil was modified to its minimum value (5 °C) while the power was set at maximum. In this way, the regulation is strongly oscillated to its set-up value.

2.5.4 Scope of the investigations

with a view to extending the methodology to other equipment, it is important to underline the scope of the investigation. The experimental dataset concerns the above-mentioned Air Handling Unit (AHU) with supply and exhaust ducts. An air-to-air heat exchanger links both ducts to heat incoming air from the outside in winter. The data are based on similar BAS sensors. Several hard, soft and operation faults were studied, as detailed in Table 2. The focus was on the AHU and not on the zone-level equipment or sensor anomalies.

3 Results

For the sake of compactness, all the data generated for this article are not presented in this section.

3.1 Data set for normal operation

The two fans were operated continuously and the temperature was the result of normal use of the system in both summer and winter campaigns.

Figure 6(a) shows the power of the supply air fan and the exhaust fan. Both fans were continuously powered during the test with a similar power value. Figure 6(a) also presents the air drop on the circular dampers and the associated airflow in the inlet and outlet duct, respectively. This highlights the fact that the air circulates normally and is well-balanced in the two ducts. Indeed, the average supply and exhaust airflows were 124.0 $\mathsf{m}^3\,.\,\mathsf{h}^{-1}$ and 125.0 $\mathsf{m}^3.\mathsf{h}^{-1}$, respectively. The difference between the airflow was less than 1%. Figure 6(b) presents the four recorded temperatures in the system: supply air, outside air, return air and exhaust air. The system was operated in a summer period, with an outdoor temperature of around 38 °C. It was in steady state and nominal operation since the supply air was cooled by the heat exchanger using the indoor air. The efficiency of the exchanger is given in Figure 6(c) and scales with 75%. Additional dataset were produced for variable fan speeds.

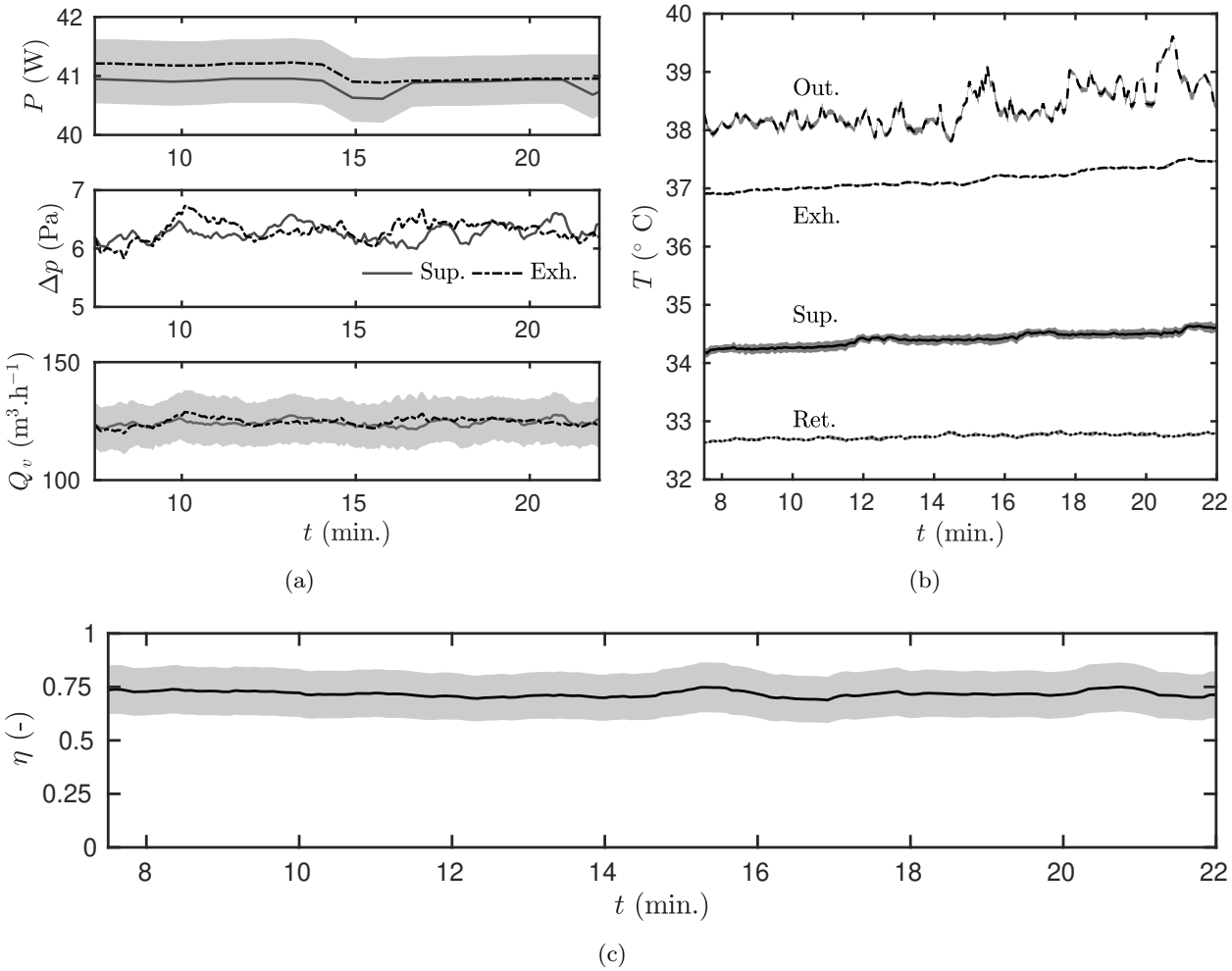

Figure 6. *Set of experimental data for a nominal operation of the system at low speed in the summer configuration.*

A very similar analysis of Figure 7 can be carried out for the winter campaign. Defrost were activated when the outside temperature was below 5 °C. The heat coil also worked normally since the temperature

after the heat exchanger increased from 10 to 26 °C. The coil consumption spanned 150 to 500 W. The system was run in steady state with an exchanger efficiency that was a bit lower than for the summer (around 60 %).

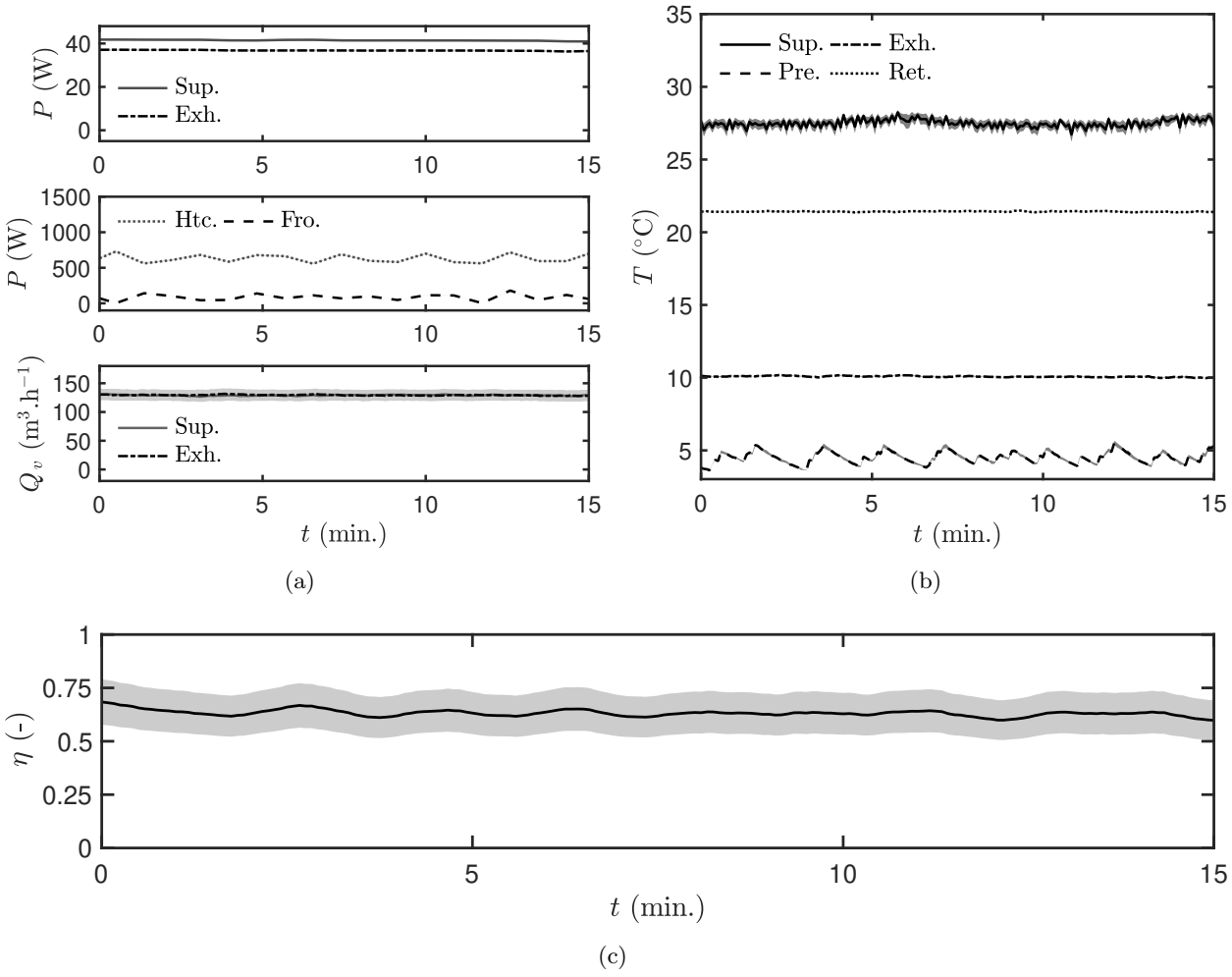

Figure 7. *Set of experimental data for a nominal operation of the system at low speed with a defrost coil in winter the configuration.*

3.2 Data set for a fan failure

3.2.1 Supply fan failure

The experimental default set presents the breakdown of a supply fan. As noted in Figure 8, the default appeared at $t = 13$ min after a brief period of normal operation. At this time, the supply fan power decreased to zero while the exhaust fan supply functioned normally. The breakdown of the supply air fan led to an immediate drop in the airflow in the inlet air duct. The default is also highlighted on the temperature variations in Figure 8(b). The supply, exhaust and return air temperatures were in steady state before $t = 13$ min. When the default appeared, these temperatures were in a transient regime. After a sufficient time, $t \simeq 25$ min, the system reached another steady state, corresponding to a default of the airflow in the supply duct. It should be noted that the measurement uncertainty increased for the outdoor temperature and the supply air temperature when the default appeared. Indeed, the air in the duct was not well mixed and some stratifications appeared. This experimental set is qualified as a default since it induces a sanitary problem in the building. There is a lack of clean fresh air in the room. Moreover, the

system efficiency is deteriorated as shown in Figure 8(a). It decreases from almost 70% to 0 when the fan failure occurs.

In the supplementary material, additional data are also proposed for a supply fan failure with a higher airflow.

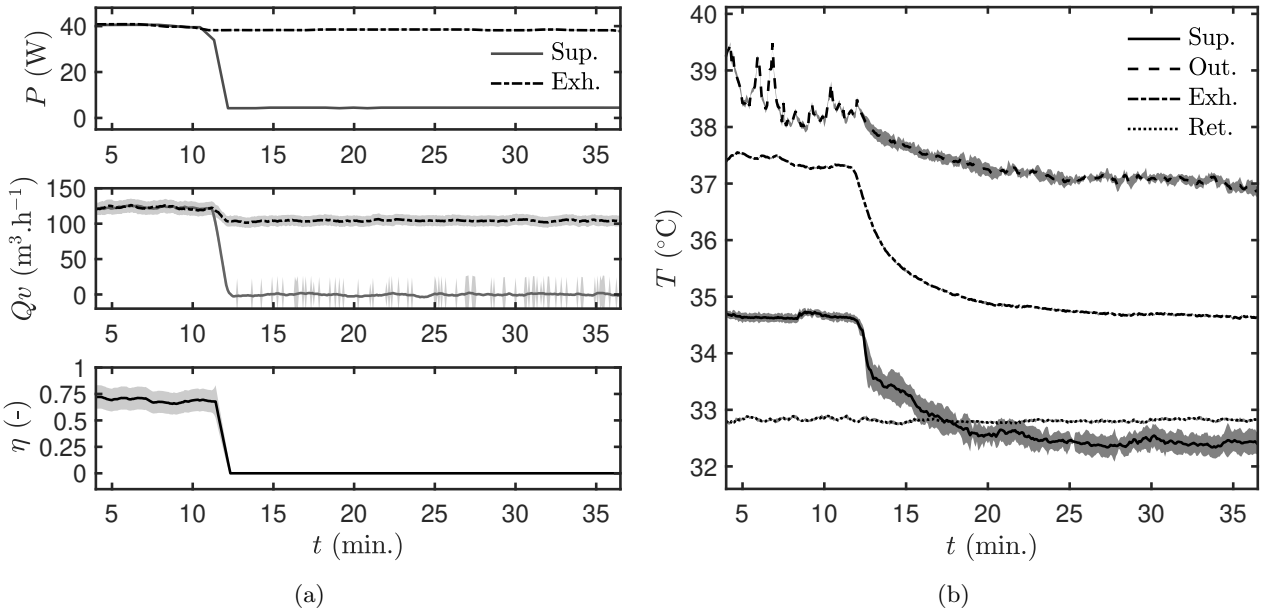

(a) (b)

Figure 8. *Set of experimental data for a supply fan failure at low speed.*

3.2.2 Exhaust fan failure

A dataset was produced for an exhaust fan failure using the fan power commutator. Similarly, a default was forced after a period of nominal operation. The measurements are presented in Figure 9. The power of the exhaust fan declined at around $t = 14\,\mathsf{min}$. The supply fan was still in normal use. The observations are very similar to those for the supply fan failure. Figure 9(a) shows that air circulation in the exhaust duct stopped as soon as the power to the fan is was cut off. The temperature was different from the supply fan failure presented in Figure 8(b). For $t \leqslant 14\mathsf{min}$, the supply air temperature was at a level between that of the outside air and the return air. The heat exchanger is functioned normally. When the exhaust fan failed, there was no cooling in the heat exchanger. Thus, for $t \geqslant 14\mathsf{min}$, the supply temperature increased until it reached the outside air temperature. The measurement was smooth since the sensor is located inside the thermal zone. This is corroborated by an analysis of the heat exchanger efficiency presented in Figure 9(a). The fault created a decrease in the heat exchanger efficiency, which went from 76% % to 0%. A short increase of over 100% can be noted before it vaniched, which is due to the short recording time step. When the power to the fan is cut, the airflow decreased and therefore the denominator of equation (2) increases. This fault is qualified as hard since it induces an inability of the system to operate. However, in contrast to the supply fan failure, it did not lead to a sanitary problem due to a lack of air exchanges.

3.3 Data set for nominal operation with the use of a bypass

This section provides an experimental dataset for a normal operation of the bypass at both high and low fan speeds.

First, the bypass was activated for maximal airflow in the ducts. Figure 10(a) shows the bypass damper power. The two fans were suitably operated at their maximal power during the whole test. At $t = 15\,\mathsf{min}$, the damper position changed, forcing the airflow to bypass the heat exchanger. As noticed, the airflow was still well balanced in the ducts, at around 200 $\mathsf{m}^3.\mathsf{h}^{-1}$. Figure 10(b) shows the temperature. The return

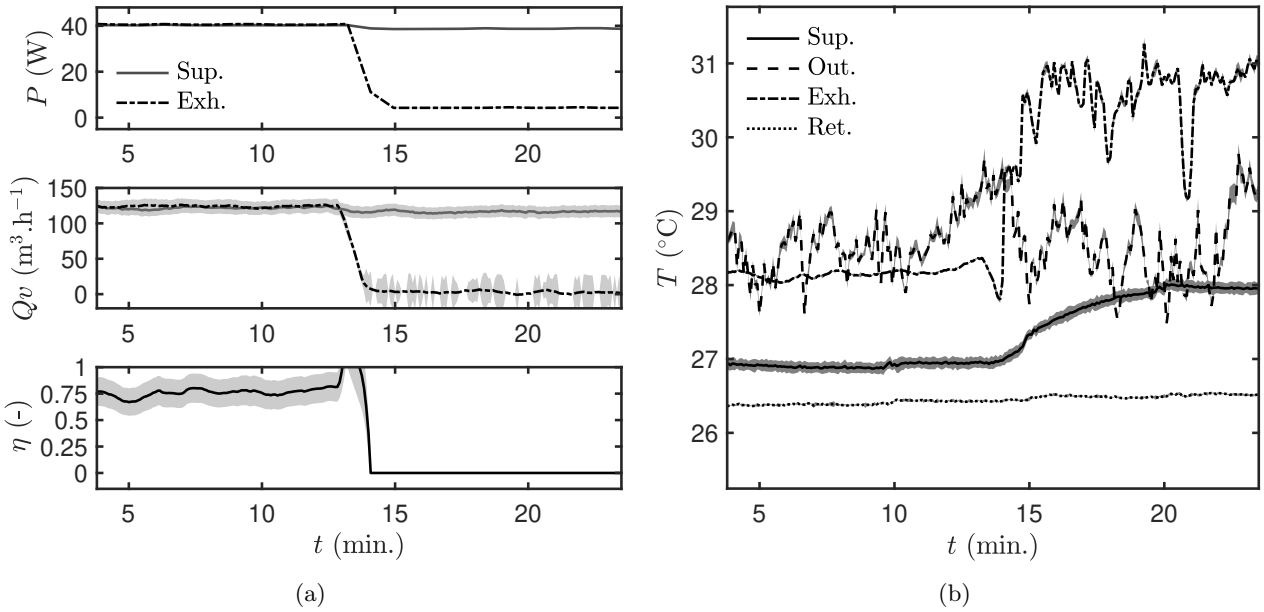

Figure 9. *Set of experimental data for an exhaust fan failure at low speed.*

temperature, corresponding to that of the inside room, was very high, at around 25.2 °C. It was also higher than the outside temperature of 21 °C. These are suitable conditions for free cooling. Thus, the bypass damper was powered at $t = 15$ min. As a consequence, the heat exchanger was no longer used and the supply air decreases almost instantaneously by 1 °C. Conversely, the opposite phenomenon was observed for the exhaust temperature. As shown in Figure 2, the return air temperature was upstream from the exhaust air temperature. Thus, the fact that the exhaust temperature approached that of the return air also indicates that less energy was exchanged in the heat exchanger. Figure 10(a) shows the heat exchanged in the system. This confirms that there was less heat gain in the heat exchanger when the bypass was opened. This did not have a directly appreciable impact on the inside air because of the volume of air in the room.

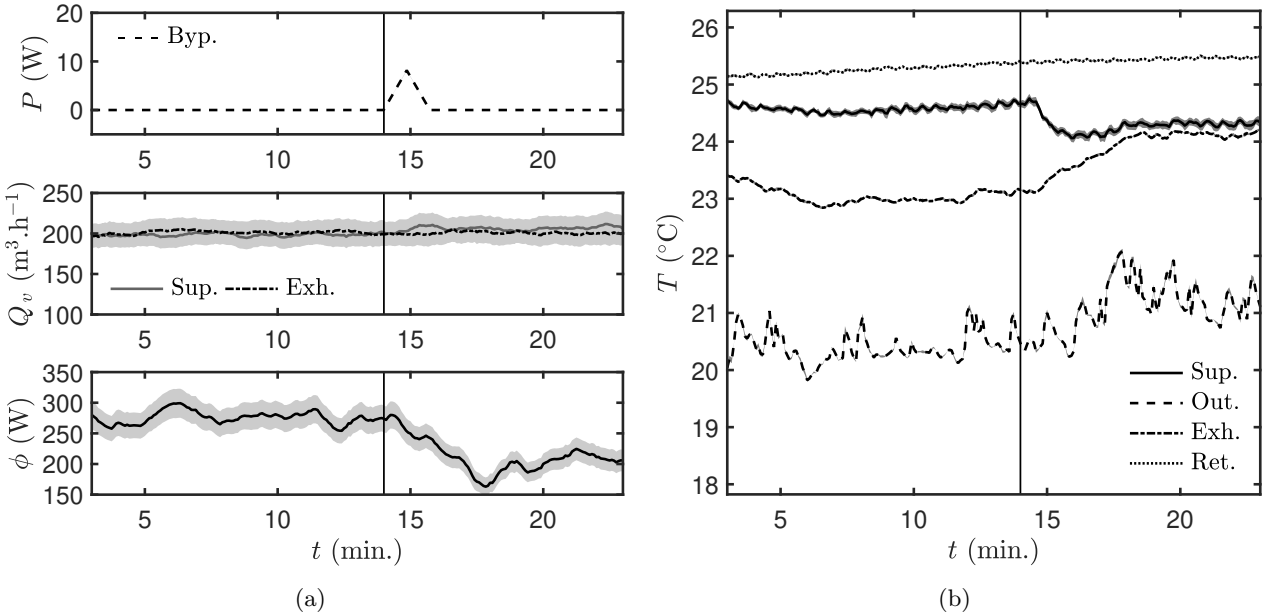

Figure 10. *Set of experimental data for a normal operation using the bypass at an initial high fan speed.*

The second set of data corresponds to a normal operation with the bypass activated at an initial low fan speed. The dataset is presented in Figure 11. In Figure 11(a), it can be seen that when the damper was activated, the airflows in both ducts also increase. As a consequence, the electricity consumption of the fans also rose. The temperature variation show in Figure 11(b) was very similar to our observations for high speed. The inside room air temperature was higher than the outdoor temperature during the whole test, corresponding to a positive situation for free cooling. When opening the bypass, a change was noticed in the supply and exhaust air temperature. The primer tended toward the outside air temperature and the exhaust air to the indoor air temperature. Theoretically, with a sufficiently long time, the supply air temperature should become equal to the outside air temperature, and the exhaust air temperature to the indoor air temperature. These changes are due to the reduction of the heat transfer when the bypass is opened. To highlight the decrease in heat exchange, Figure 11(a) shows the difference between the outside and supply air temperature. There was a loss of 1 °C between the two states.

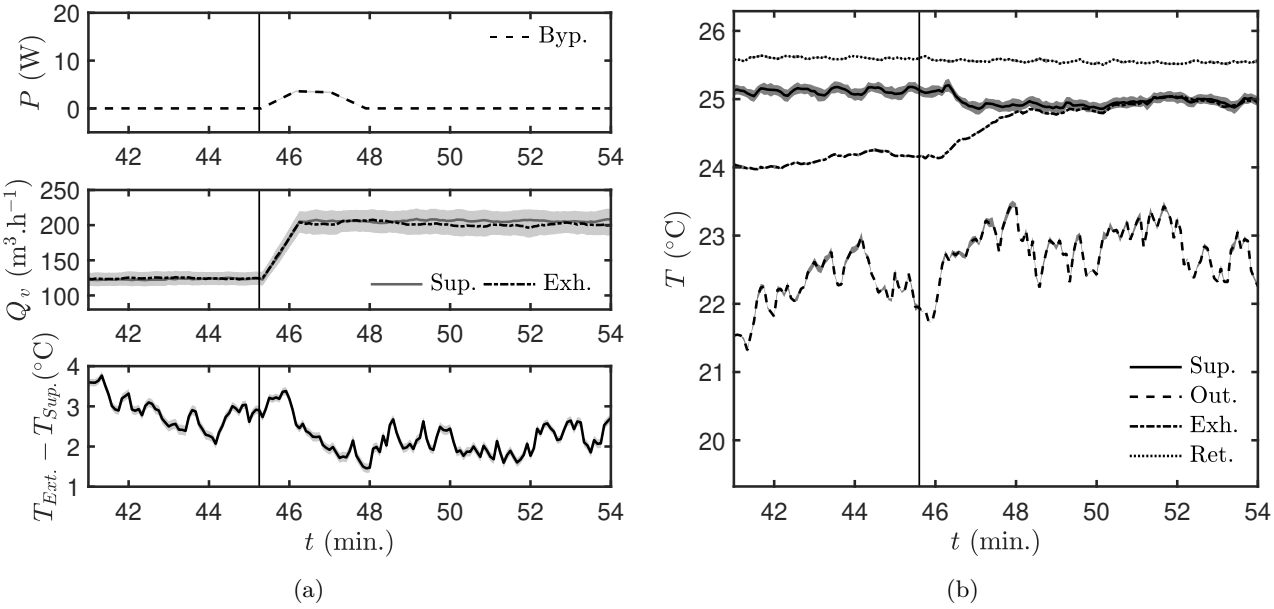

Figure 11. *Set of experimental data for a normal operation using the bypass at an initial low fan speed.*

3.4 Data set for a bypass failure

After presenting the nominal use of the bypass, a dataset for a defective operation are now introduced. Three of the six possible faults identified are presented in the following section: two for high fan speed and one for low fan speed.

3.4.1 Initial high fan speed

Three defaults can occur with an initial high fan speed. The first is when the bypass is not activated. The experimental dataset is presented in Figure 12. In Figure 12(a), the power of the two fans was constant at the highest value. However, the bypass damper energy consumption was constantly null indicating a failure of the system. The supply and exhaust airflows were nominal and well balanced, as noted in Figure 12(a). The temperature variation is presented in Figure 12(b). It is clear that a free cooling potential existed but was not used. The outside temperature was almost 5 °C below the return temperature corresponding to the air temperature in the inside room. In such conditions, the bypass should be activated to cool the air in the room. Figure 12(a) presents the gain of the heat exchanger. During the test, it remained constant at around 250 W. This reinforces the idea that it is a faulty state compared to the influence of the bypass activation in Figure 10.

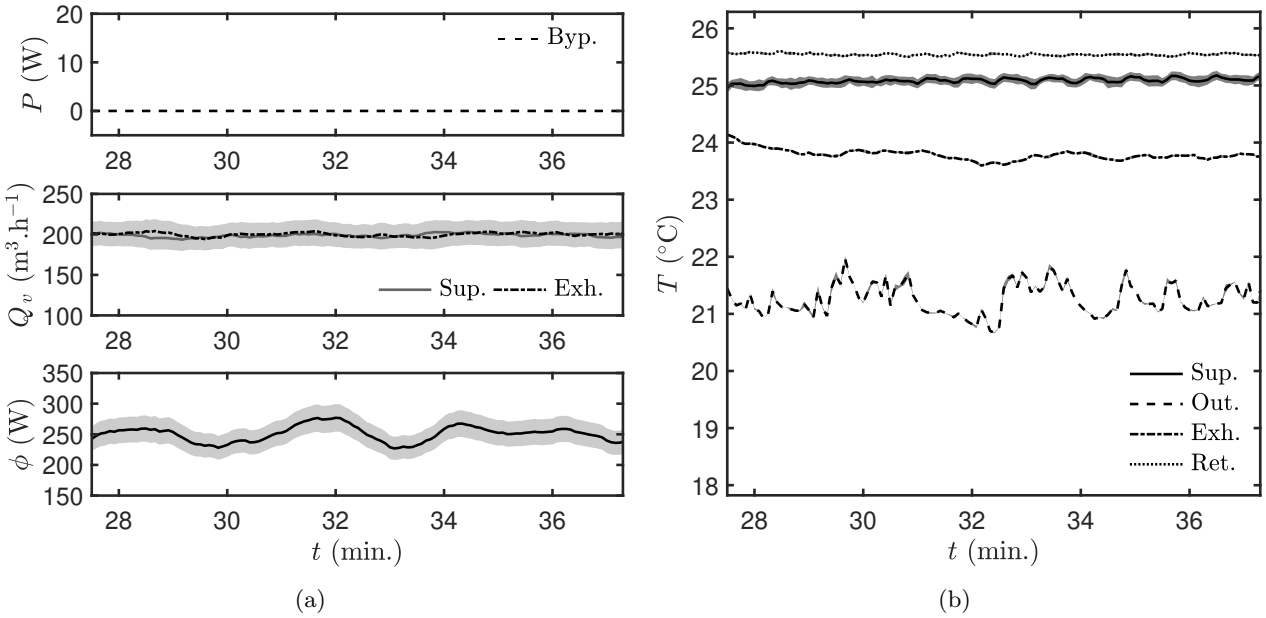

(a) (b)

Figure 12. *Set of experimental data with a bypass failure at an initial high speed fan: the bypass was not activated while the airflow was working.*

Conversely, the second default happened when the bypass was activated but the airflow reduced. As shown in Figure 13(a), the bypass damper was turned on at $t = 40$ min. At the same time, this also shows that the airflow in both ducts decreased. The power of the fans also dropped down. The temperature variation in the system is presented in Figure 13(b). A free cooling of the building was possible but, due to the default, less fresh air was injected into the building. Thus, even if the bypass is opened, cooling is slower compared to the nominal case. There was a smooth transition of the system as shown in Figure 13(a).

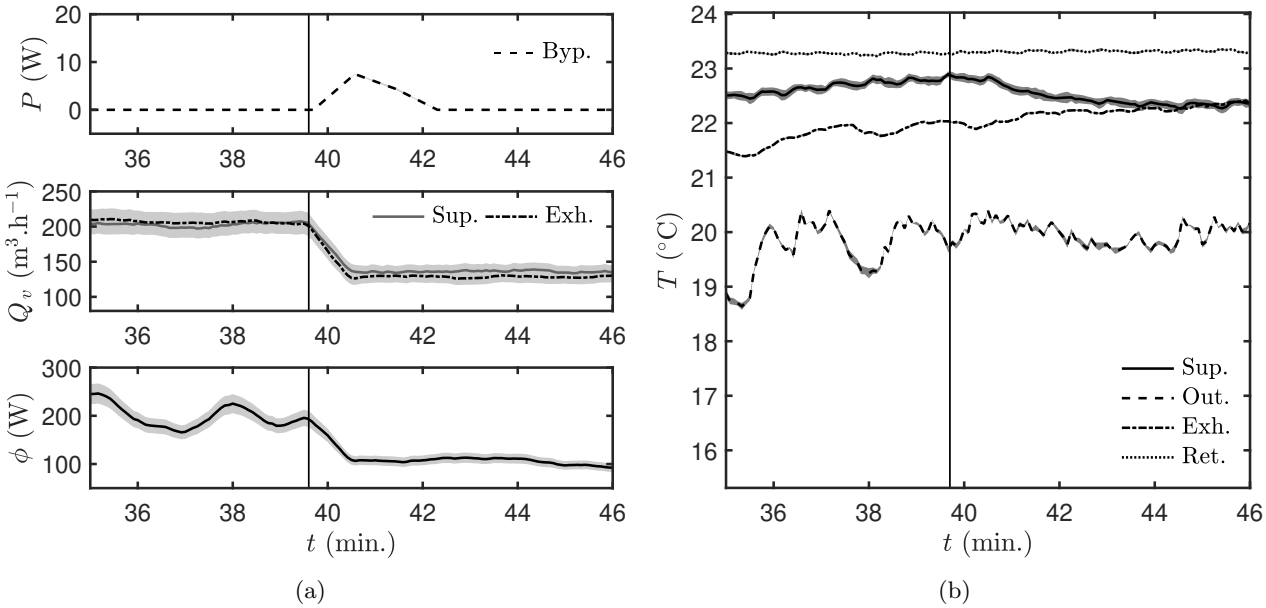

(a) (b)

Figure 13. *Set of experimental data with a bypass failure at an initial high speed fan: the bypass was activated while the airflow was reduced in the ducts.*

The last fault case regarding high fan speed occured when the airflow was diminished and the bypass

damper was not activated. For the sake of compactness, the experimental dataset for this last case is presented in the supplementary files.

3.4.2 Initial low fan speed

A bypass failure can also occur at an initial low fan speed. Three defaults are possible for the low speed. For the sake of compactness, only one is presented here, the other two are provided in the supplementary files. The operation default presented here appeared when the bypass damper was not opened while the airflow remained at a low level. Figure 14(a) shows that the bypass was not activated during the test. Furthermore, the airflow did not vary, suggesting that the power of the two fans remained constant at the low level. The analysis of temperature in Figure 14(b) shows that there were favourable conditions for free cooling. There was no significant change in the dynamics of the fields. Figure 14(a) also gives the variation with time of the heat exchanger efficiency. Since the bypass was not working, there was no significant modification in the heat exchanged. Indeed, the efficiency remained almost constant in during nominal functioning.

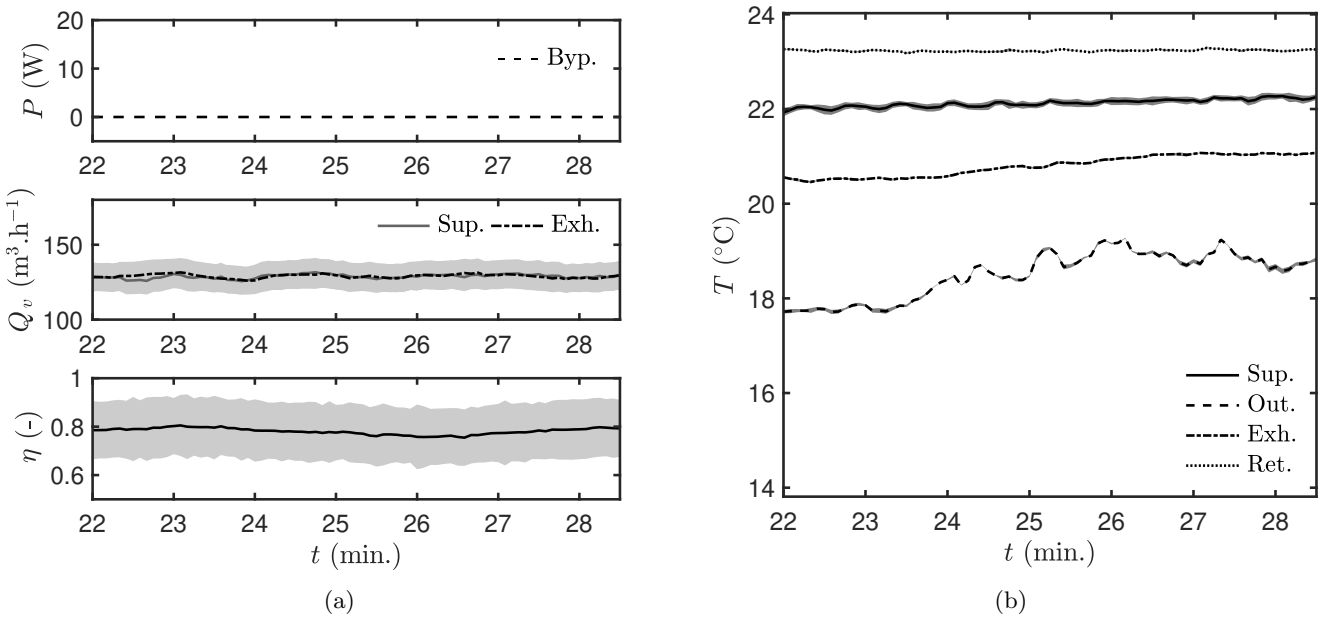

Figure 14. *Set of experimental data with a bypass failure at an initial low speed fan: the bypass is not activated and the airflow did not increase.*

3.5 Data set for a filter fouling

For this experimental dataset, it should be remembered that the bypass was no longer used and the conditions were not favourable for free cooling. Here, the impact of filter fouling on the airflow and thus the efficiency of the heat exchanger, was investigated. Each supply and exhaust duct filter was obstructed separately in a specific test. The case presented occured when the filter placed on the supply air duct was clogged. An additional set of data is provided in supplementary materials for the congestion of the extracted air duct.

Figure 15 shows the variation in the airflow and the efficiency with three filter clogging cases. It can be seen in Figure 15(a) that the value of the supply airflow decreased when filter fooling increased. It went from 124.6 $\pm$ 2% $\mathsf{m}^3.\mathsf{h}^{-1}$ for no obstruction to 118.8 $\pm$ 2% $\mathsf{m}^3.\mathsf{h}^{-1}$ for an obstruction of 80% of the filter. This corresponds to a reduction of 5% of the initial nominal airflow. Furthermore, in such a default case, the airflow in the two ducts was no longer well-balanced, which induced unexpected air circulation in the building and a higher energy consumption by the fan. As a consequence, the efficiency of the heat exchanger

decreased significantly with filter fouling, as shown in Figure 15(b). A reduction of 25% of the efficiency was observed for a fouling of 80%.

Figures 16(a) and 16(b) present the change with time of the average airflow and heat exchanger efficiency according to clogging percentage. By fitting an empirical model, an increase of 10% of fouling induced a reduction of 2.5% of the efficiency. Figure 16(a) also reveals that the minimal standard requested value of air exchanged was not reached for an obstruction higher than 60%. Thus, an additional sanitary fault appeared when the minimal air exchange value of 120 $\mathsf{m}^3.\mathsf{h}^{-1}$ was not respected.

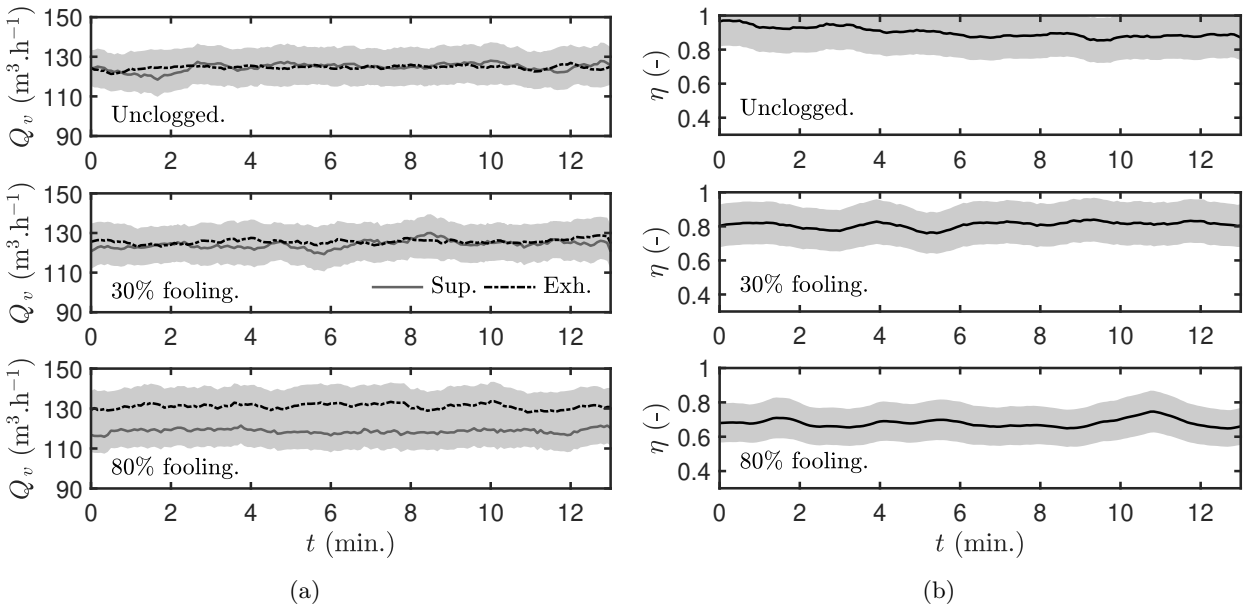

Figure 15. *Set of experimental data for the supply duct filter fooling.*

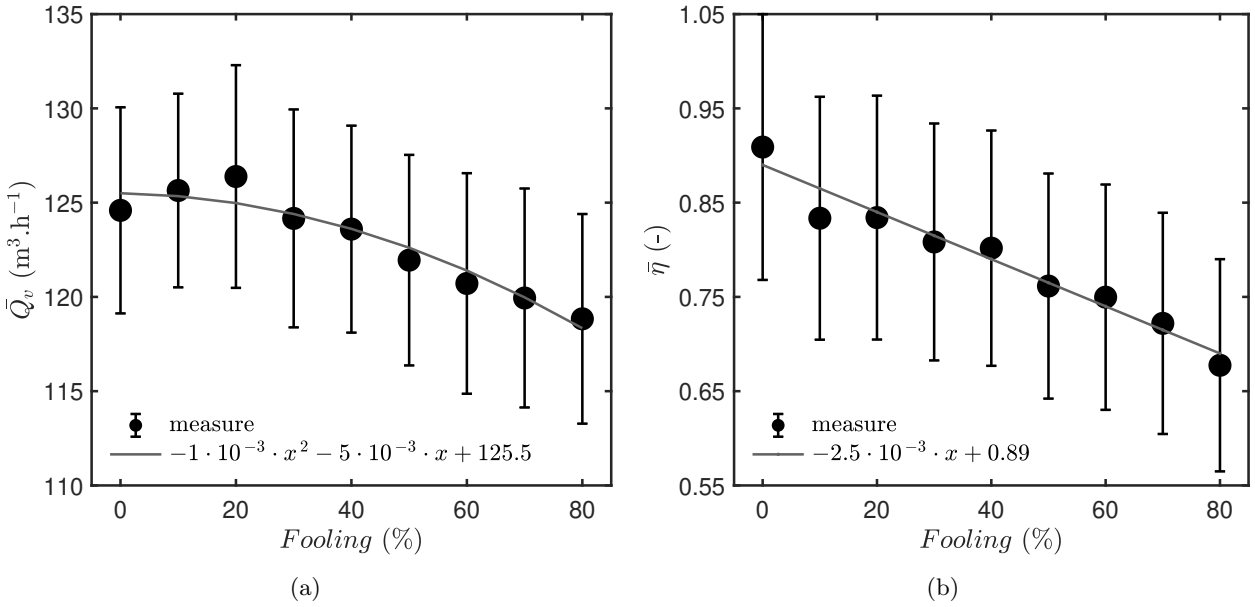

Figure 16. *Evolution of the averaged supply duct air flow* (a) *and the heat exchanger efficiency* (b) *according to the fouling.*

3.6 Data set for duct obstruction

The next experimental dataset is for an obstruction of each of the four ducts. For the faults presented in the following section, the fans were operated at low speed. Figure 17 presents the airflow in the ducts during the four obstruction cases. The two cases dealing with the supply duct are presented in Figure 17(a) and the cases on the exhaust duct in Figure 17(b). Regarding the case of the obstruction of a fresh air duct, two important elements can be highlighted. First, when the damper is closed during the test, the airflow in the duct sheltering the damper decreased. At the same time, the airflow in the exhaust duct increased. Thus, for the obstruction of the fresh air duct, damper closure induced both a reduction in the supply airflow and an increase in the extraction duct. A similar trend was also observed in the fan power data, but this was very slight and withing the margin of error. Very similar observations were made in the case of an obstruction of the expelled air duct, in Figure 17(b).

Figure 17(a) also shows the variation in airflow in two ducts for an obstruction in the blow-in air duct. After obstruction, the pressure loss increased leading to a fall in airflow in the duct. A slight reduction in the exhaust airflow was also noticed. In this case, the fault induced a sanitary issue since the fresh air supply in the room was below the recommended value of 120 $\mathsf{m}^3.\mathsf{h}^{-1}$. A similar conclusion can be drawn when the expelled air duct is obstructed.

The same test was conducted on a system with the fans working at high speed. The results are provided in the supplementary material.

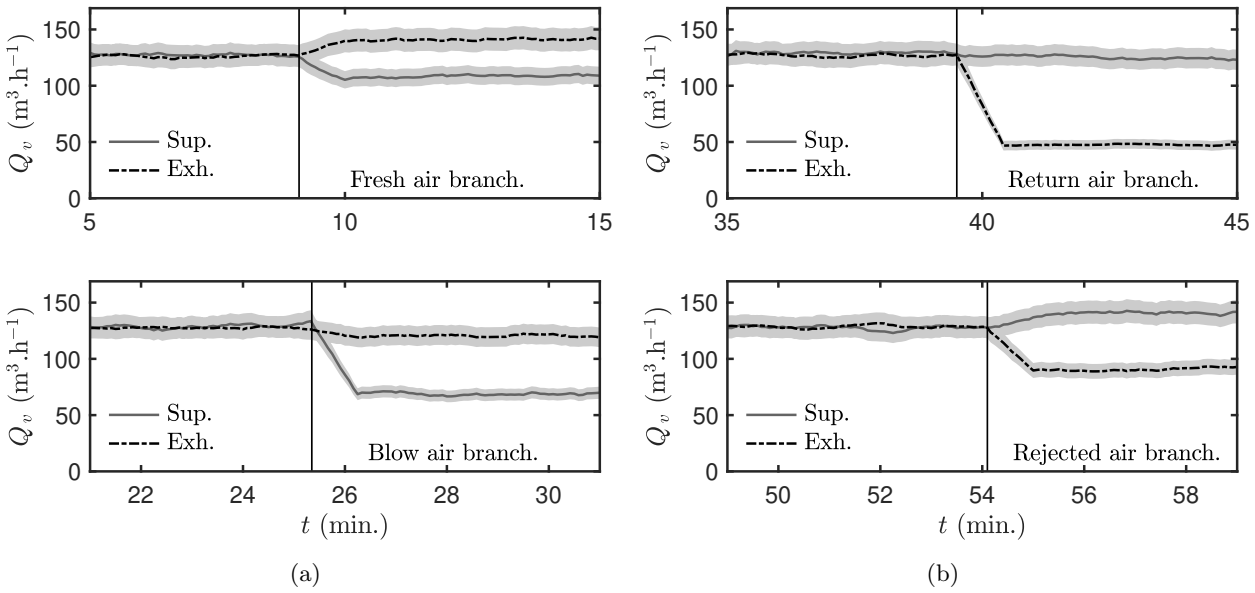

Figure 17. *Set of experimental data for supply* (a) *and exhaust* (b) *ducts obstruction at low speed.*

3.7 Data set for fan belt breakdown

Fan belt breakdown is a usual fault that stops the airflow in a duct. It is similar to a fan failure fault, although, the electrical motor is still operating, consuming energy and maintaining a nominal function. However, the rotation is not effective and no airflow is generated. An experimental dataset is provided for both a supply and exhaust fan, at high and low speed. For the sake of compactness, only the results regarding high speed are presented here, the low speed results are provided in the supplementary material.

In Figure 18, supply fan belt breakdown appeared at $t = 42$ min. The airflow in the supply duct ended abruptly, while in the exhaust duct continued at its nominal level. As a consequence, heat exchanger efficiency dropped to zero since Eq. (2) depends on the airflow. It can be noted that the power provided to the two fans remained constant, indicating that the motors were still operating. This simulates a fan belt

breakdown. Figure 18(b) presents the temperature during the test. The supply and exhaust air temperatures changed considerably after the airflow stopped.

The next case is for an exhaust fan belt breakdown. The experimental dataset is presented in Figures 19(a) and 19(b). The airflow dropped in the exhaust duct, suggesting a decrease in efficiency, while both fans maintained a nominal energy consumption. As for the previous case, the temperature of the supply and exhaust air ducts was modified.

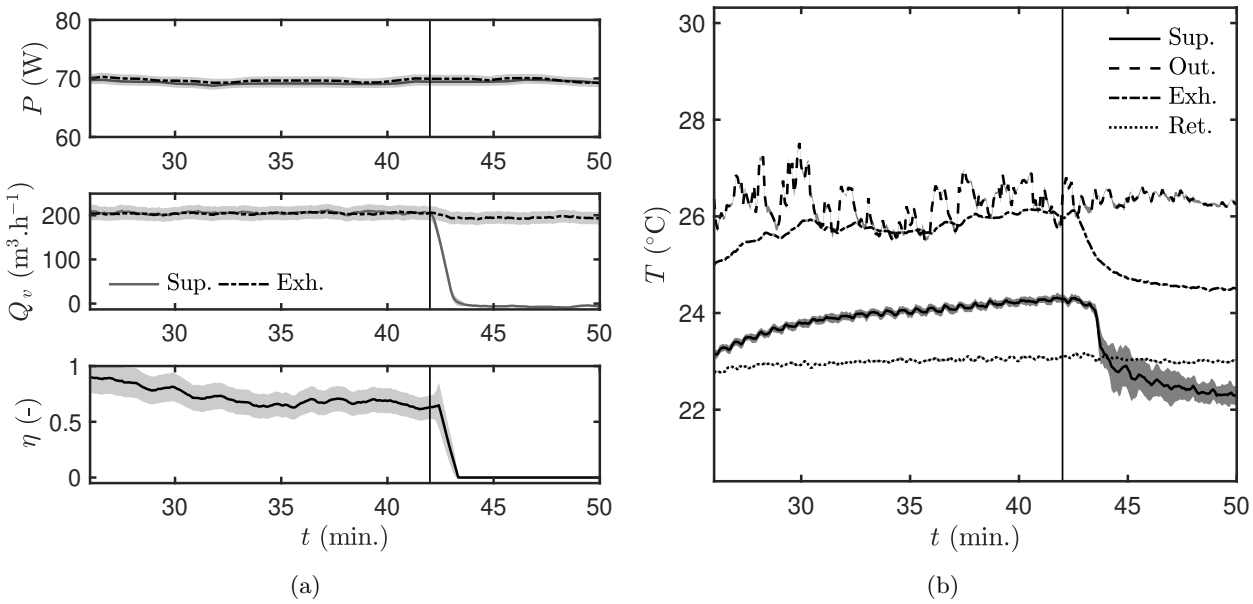

Figure 18. *Set of experimental data for a supply fan belt breakdown at high speed.*

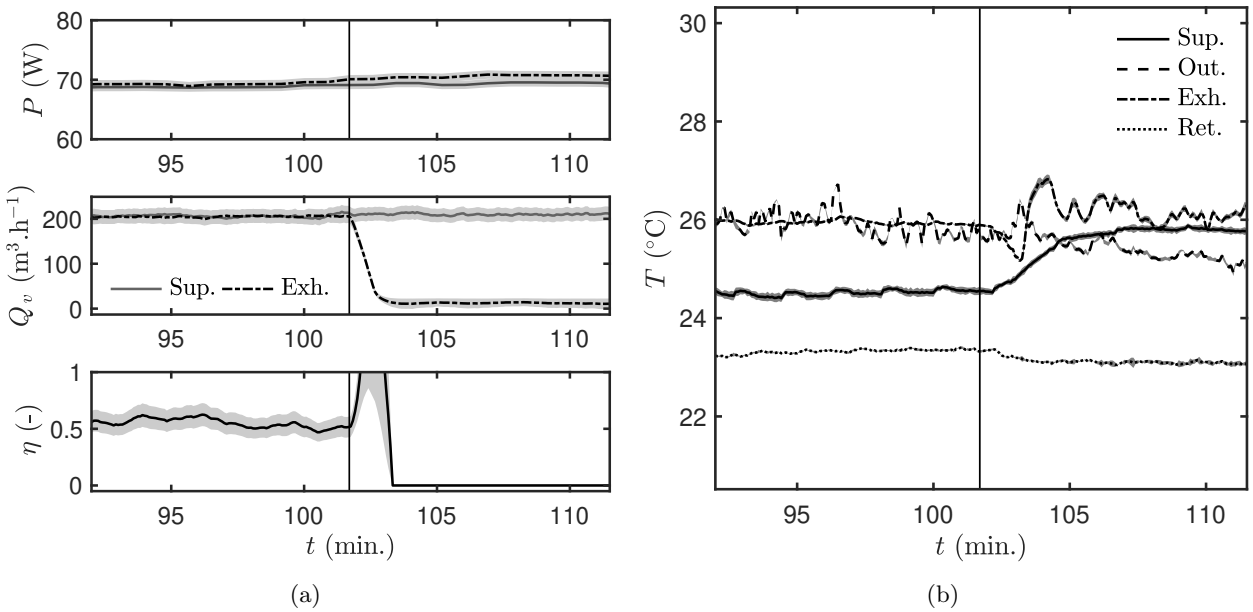

Figure 19. *Set of experimental data for an exhaust fan belt breakdown at high speed.*

3.8 Bypass damper failure

This dataset concerns an obstruction of the bypass damper. The fault was generated in a free cooling context, at both low and high speed. Only high speed is presented here. The low speed data is available in the supplementary material. Figure 20(a) shows that the airflow remained at the highest level during the whole test, even when the bypass was activated. The bypass damper received an electrical impulsion to open, at $t = 31$ min since there was a free cooling potential. However, it was mechanically blocked and could not be opened to let the airflow through. It is worth mentioning the bypass power is non-null after activation because the damper cannot touch the contactor that stops the energy supply. The heat exchanger efficiency remained stable because the bypass damper was not open. Figure 20(b) shows that the air temperature in the system was not perturbed during the test, remaining in steady state.

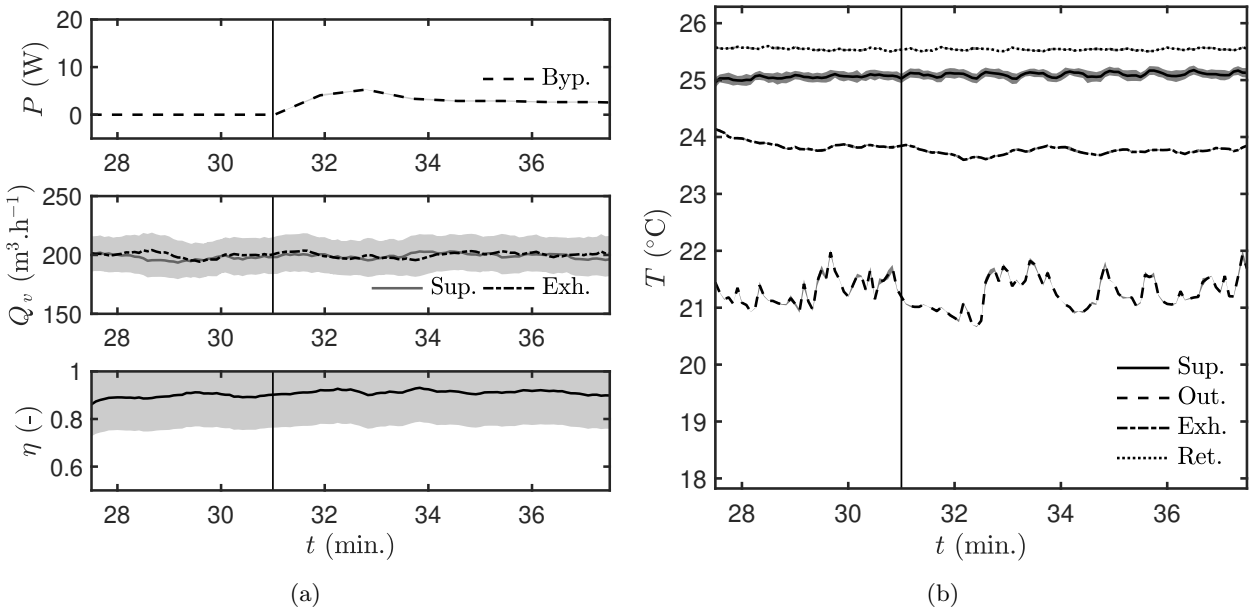

Figure 20. *Set of experimental data for a bypass damper obstruction at high speed.*

3.9 Defrost and heat coil failure

In this case, the defrost coil fails while the system is operating in nominal condition with a need to pre-heat the outside air. Figure 21(a) demonstrates that the fans were working normally with a constant and balanced airflow. As remarked, the supply fan power consumption was constant during the test. Nevertheless, at $t = 0$ the power consumption of the defrost coil ended abruptly. Analysis of Figure 21(b) is consistent with these results. The supply temperature was constant with an internal temperature of 21 °C. The pre-heating temperature was around 5 °C until $t = 0$. With defrost coil failure, the pre-heating temperature decreased to the level of the outside temperature. The minimum temperature required in the heat exchanger to avoid condensation is not guaranteed. Figure 21(c) gives the heat flux provided by the defrost coil computed according to Eq. (4). The flux remained stable until the failure and then decreased slowly. A very similar dataset is provided for a heat coil failure with the experimental results provided in Figure 22.

3.10 Defrost coil regulation

The last dataset concerns defrost coil regulation. Here, the PID regulation is not working accurately. Figure 23(a) shows the variation in the power consumption of the fans and coils as well as airflow. The power consumption and airflow were constant for the fans. However, the power consumption of the defrost coil varied between 0 and 1000 W due to bad regulation. Figure 23(b) also shows that the pre-heating

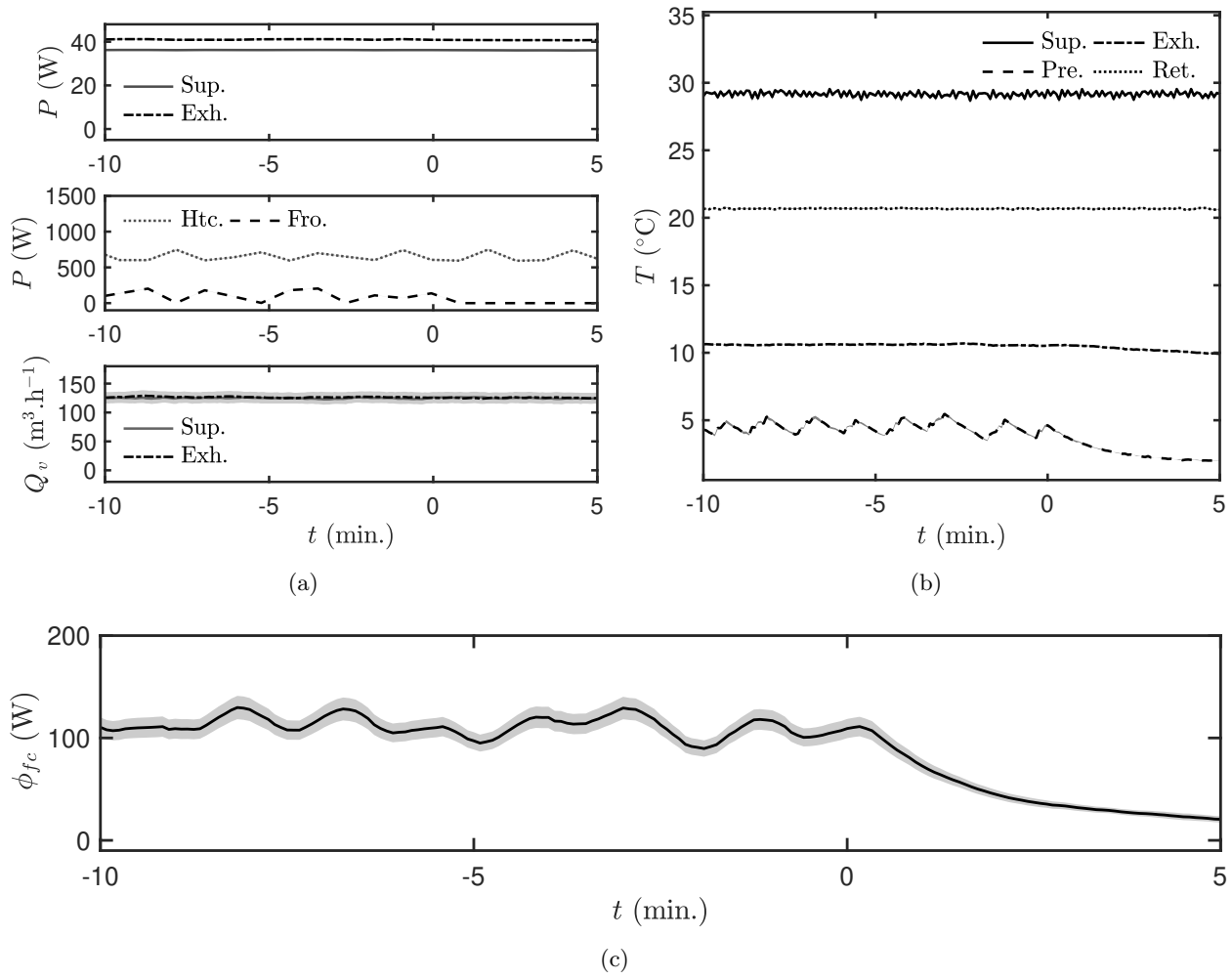

Figure 21. *Set of experimental data for defrost coil failure.*

temperature was not constant at all; it varied dramatically, corresponding to the instant when the coil was turned on, and was not stable at 5 °C as expected with the set-up. Similarly, the efficiency of the heat exchanger also varied between 0 and 60 %, as noted in Figure 23(c).

4 Further remarks and conclusion

Before giving some general conclusion based on our dataset, several remarks can be made regarding the experimental results. As can be noticed on several Figures, as for instance Figure 8(b), the temperature uncertainty increased with a decrease in the airflow. This is probably due to a temperature stratification or just a non-uniform temperature distribution in the duct. It should be remembered that the temperature was measured by physical redundancy with two thermocouples. However, it is important to note that the maximal standard deviation of temperature remained under 0.3° C.

The heat exchanger bypass of the system may not achieve its function totally. Actually, the bypass is made of a little trap above the heat exchanger, which allows a preferential path for the air but is not a complete bypass of the heat exchanger. For instance in Figure 10(b), the supply temperature was reduced after the bypass was opened but was still relatively different to the outside air temperature (around four degrees). The remaining difference highlights the fact that part of the supply air is always heated in the exchanger. This phenomenon can also be observed in Figures 11(b) or 13(b). It should be underlined that this corresponds to the product line provided by the supplier. Thus, it represents a real system set-up in a

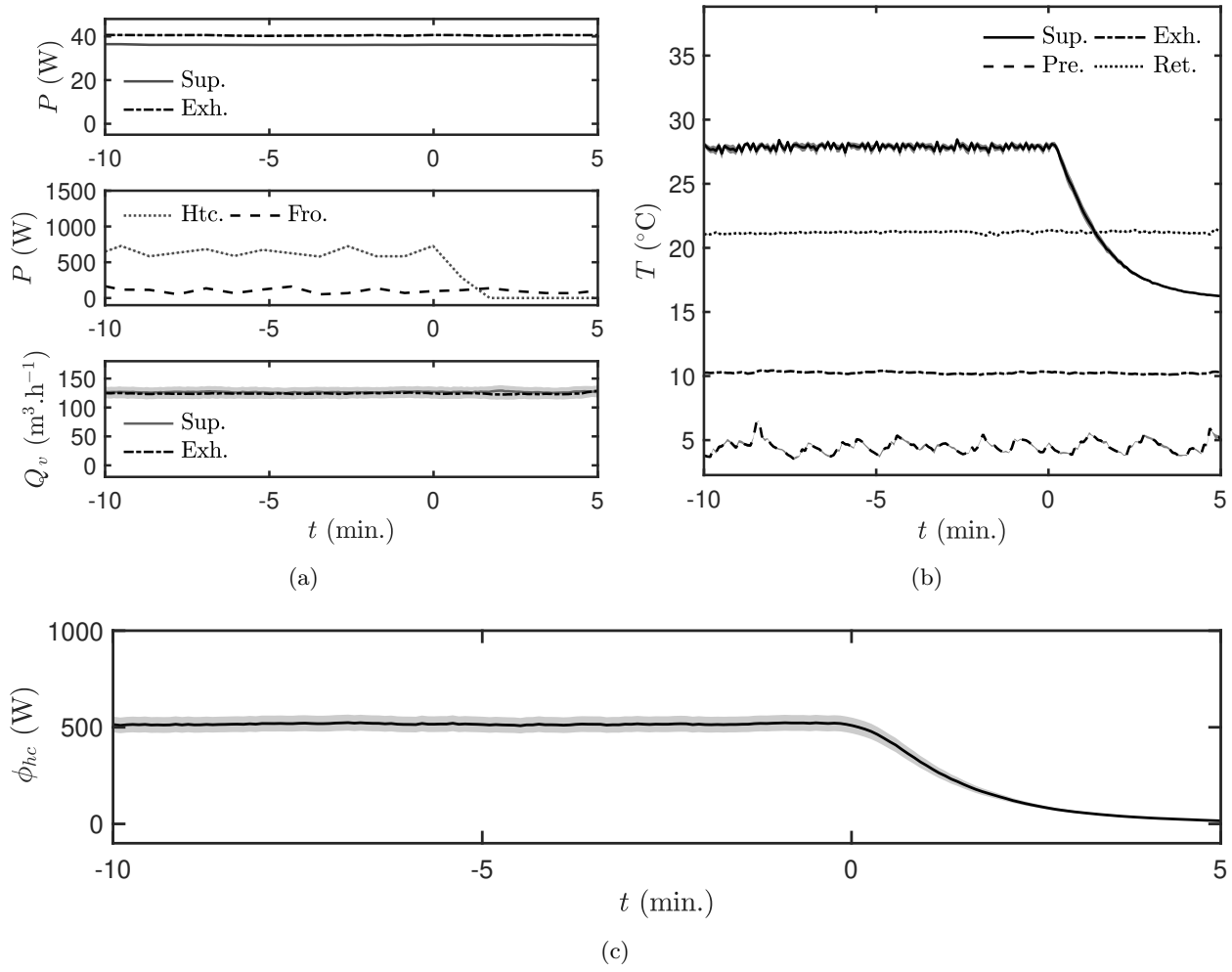

Figure 22. *Set of experimental data for heat coil failure.*

building.

The airflow may vary in surprising manner in Figures 17(a) and 17(b). When the damper is closed, one airflow decreased, as expected, while the other increased. This behaviour seems to be due to the DFX AHU system itself. There is a lack of permeablity of the inside air in the system, causing unwanted air transfer between the two ducts when the pressure loss increases. Again, this represents a real system in use.

Regarding the filter fouling protocol, the authors are aware that the surface obstruction of the filter used to represent filter clogging is not representative of the physical reality. The behavior inside the filter, like the velocity field, can significantly differ from a real fouling and surface percentage obstruction of a filter. However, the main objective was to induce a reduction in the airflow and efficiency due to filter problems. Indeed, the impacts on these two physical quantities are the result of filter fouling and the topic of this study is fault detection. Moreover, it would be more interesting to have data of a continuous increase in the filter fouling rather than discrete values. However, no experimental protocol allows such a continuous generation of filter fooling. Thus it was decided to provide data under different percentages of filter clogging. Moreover, the filer clogging phenomena generally appear over several months or years of operation in normal cases. These issues will be investigated in the our future work.

It is important to note that even though human interaction with the building and the inside space has an impact on the indoor conditions, it has not been specifically represented during the experimental tests. Indeed, the system studied has to respond appropriately to inputs (like inside or outside temperature), with controllable outputs (such as blown temperature or the bypass damper position), regarding the condition targeted by the operation or maintenance staff. Thus, human activity (regarding thermal and moisture

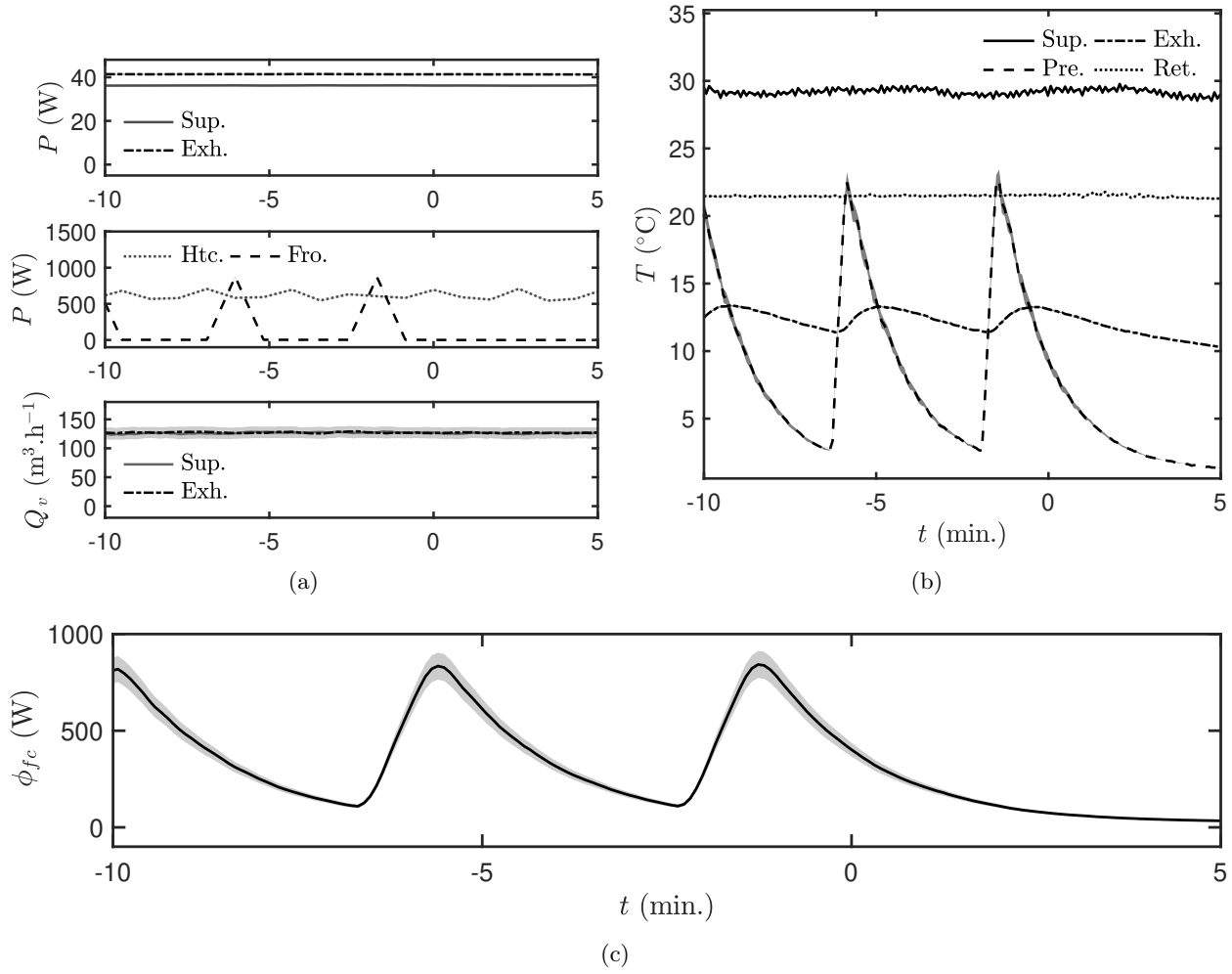

Figure 23. *Set of experimental data for a defrost coil regulation at low speed.*

generation) is an influential parameter for the internal conditions (solar irradiation, for example), which is already a controlled variable. Note that faulty human actions are dealt with in the clogging of an air vent.

Examples of the use of such experimental data for FDD in real projects can be found in the literature. Two recent studies may be cited since they are based on the same AHU equipment. In [46], a multivariate statistics method was employed to elaborate a map of the commissioning of the equipment. One year of experimental data were collected from the automation system of an office building. These maps enables a fast and understandable detection of nominal and faulty operations. In [47], a qualitative based FDD tool using dimensionality reduction was developed and its reliability was evaluated in terms of the experimental dataset provided in this work.

To summarise, this study provides experimental datasets for an AHU system. The datasets correspond to both nominal and faulty operations of the system. Nine different non-exhaustive faults were investigated, for two regimes of airflow and for each component. A total of 6 nominal operation datasets and 46 faulty operation datasets were generated. These data are provided with uncertainties in a semi-controlled room with a thorough experimental design representative of real building monitored by a BAS in both summer and winter configurations. Without getting into a debate on the merits of existing building data and experimental data, our datasets are reliable for the following reasons. *(i)* The experimental protocol and the (semi-)controlled room reduces the unknown events and maximizes the accuracy of the recorded cases (the faults and the nominal operation). However, field data do not fulfill this condition, yet are essential to ensure the suitability of the data for fault detection ; *(ii)* Experimental results provides values and their

associated uncertainties, making it possible to validate the appearance of a fault. Once again field and simulated measurements are rarely provided with this information; *(iii)* Experimental data represent real phenomena, whereas simulated data are marred by the model error or bias induced by the hypothesis, not to mention all the possibilities of simulation error made by the operator. They represent a real system usually employed in buildings monitored by BAS and subjected to climatic variation; *(iv)* Experimental data like field data include background noise in the measurements due to sensor precision, which is not simulated by the model, representing more closely the type of data processed by in situ FDD tools ; *(v)* Each fault dataset is associated with a corresponding nominal dataset to highlight the difference between them. The transition between nominal and fault sequences was almost continuous.
It is also important to be aware of the limitations of such a dataset; *(vi)* Experimental data generation is definitely more time consuming than simulation or field data retrieval, due to establishment of an experimental protocol, and then the generation of the data ; *(vii)* Experimental data are more expensive to produce than other data ; *(viii)* The experimental protocols used to properly represent specific faults are complex to set up. Note that the experimental dataset concerns only the above-mentioned Air Handling Unit (AHU) with supply and exhaust ducts as well as an air-to-air heat exchanger. The data are provided based on similar BAS sensors.

For all these reasons, our dataset should be useful for the community. It can be used as input samples to develop qualitative, quantitative or process history-based FDD tools and evaluate their prediction accuracy [7, 8]. Future work should focus on providing additional datasets for faulty operations.

Nomenclature

Latin letters

Symbols	Description	Units
C	Heat capacity	$[J.kg^{-1}.K^{-1}]$
k	Venturi Coefficient	$[m^3.h^{-1}.P^{-2}]$
P	Power	[W]
p	Pressure	[Pa]
Q_v	Volumetric airflow	$[m^3.h^{-1}]$
T	Temperature	[°C]
t	Time	[min]

Greek letters

Symbols	Description	Units
Δ	Difference between two values	[-]
ϕ	Heat flux	[W]
η	Efficiency	[-]
ρ	Density	$[kg.m^{-3}]$
σ	Uncertainty	[SI]

Abbreviation

Symbols	Description	Use
Exh.	In the exhaust duct	Pressure loss, airflow, equipment power, temperature
Sup.	In the supply duct	Pressure loss, airflow, equipment power, temperature
Nom.	At the nominal value	Efficiency
Out.	At the outdoor air location	Temperature
Ret.	At the return air location	Temperature

Acknowledgements

The authors acknowledge the laboratory LOCIE for the funding through the "AAP interne". This project is supported by the Interreg V France-Switzerland European Territorial Cooperation Program and has benefited from a European grant of 607 . 776, 49 € through the European Regional Development Fund (ERDF) as well as federal funds Interreg Switzerland for 150 . 001 CHF and 123 . 999 CHF for cantonal and communal aid.

References

[1] US Department of Energy. *Buildings Energy Data Book*. DR International, Ltd., 2012. 1

[2] Fu Xiao and Shengwei Wang. Progress and methodologies of lifecycle commissioning of HVAC systems to enhance building sustainability. *Renewable and Sustainable Energy Reviews*, 13(5):1144–1149, June 2009. 1

[3] Peter Warburton, K. J. Butcher, and Chartered Institution of Building Services Engineers, editors. *Building Control Systems*. CIBSE Guide H. CIBSE, London, 2. ed edition, 2009. OCLC: 934945430. 1

[4] Venkat Venkatasubramanian, Raghunathan Rengaswamy, Kewen Yin, and Surya N Ka. A review of process fault detection and diagnosis Part I: Quantitative model-based methods. *Computers and Chemical Engineering*, page 19, 2003. 1

[5] David P. Yuill and James E. Braun. Evaluating the performance of fault detection and diagnostics protocols applied to air-cooled unitary air-conditioning equipment. *HVAC&R Research*, 19(7):882–891, October 2013. 1

[6] David P. Yuill and James E. Braun. A figure of merit for overall performance and value of AFDD tools. *International Journal of Refrigeration*, 74:651–661, February 2017. 1

[7] Stephen Frank, Guanjing Lin, Xin Jin, Rupam Singla, Amanda Farthing, and Jessica Granderson. A performance evaluation framework for building fault detection and diagnosis algorithms. *Energy and Buildings*, 192:84–92, June 2019. 1, 26

[8] Guanjing Lin, Hannah Kramer, and Jessica Granderson. Building fault detection and diagnostics: Achieved savings, and methods to evaluate algorithm performance. *Building and Environment*, 168:106505, January 2020. 1, 26

[9] Z. Shi and W. O'Brien. Development and implementation of automated fault detection and diagnostics for building systems: A review. *Automation in Construction*, 104:215–229, 2019. 1

[10] Mangesh Basarkar, Xiufeng Pang, Liping Wang, Philip Haves, and Tianzhen Hong. Modeling and Simulation of HVAC Faults in EnergyPlus. *Proceedings of Building Simulation 2011: 12th Conference of International Building Performance Simulation Association, Sydney, 14-16 November.*, page 7, 2011. 2, 9

[11] Yanfei Li and Zheng O'Neill. A critical review of fault modeling of HVAC systems in buildings. *Building Simulation*, 11(5):953–975, October 2018.

[12] Ying Yan, Peter B. Luh, and Krishna R. Pattipati. Fault Diagnosis of Components and Sensors in HVAC Air Handling Systems With New Types of Faults. *IEEE Access*, 6:21682–21696, 2018. 2

[13] Suhrid Deshmukh, Leon Glicksman, and Leslie Norford. Case study results: Fault detection in air-handling units in buildings. *Advances in Building Energy Research*, pages 1–17, November 2018. 2

[14] J. Schein, S. T. Bushby, N. S. Castro, and J. M. House. A rule-based fault detection method for air handling units. *Energy and Buildings*, 38(12):1485–1492, 2006. 9

[15] J. Trojanová, J. Vass, K. Macek, J. Rojiček, and P. Stluka. Fault Diagnosis of Air Handling Units. *IFAC Proceedings Volumes*, 42(8):366–371, 2009. 2

[16] H. Burak Gunay and Zixiao Shi. Cluster analysis-based anomaly detection in building automation systems. *Energy and Buildings*, 228:110445, 2020. 2, 9

[17] H. B. Gunay, W. Shen, and G. Newsham. Data analytics to improve building performance: A critical review. *Automation in Construction*, 97:96–109, 2019. 2

[18] J. Wen and US S. Li ASHRAE, Ed. ed. Atlanta. Rp 1312: Tools for evaluating fault detection and diagnostic methods for air-handling units. Technical report, 2012. 2

[19] L. K. Norford, J. A. Wright, R. A. Buswell, D. Luo, C. J. Klaassen, and A. Suby. Demonstration of fault detection and diagnosis methods for air-handling units. *HVAC&R Research*, 8(1):41–71, 2002. 2

[20] T. Abuimara, B. W. Hobson, B. Gunay, W. O'Brien, and M. Kane. Current state and future challenges in building management: Practitioner interviews and a literature review. *Journal of Building Engineering*, 41:102803, 2021. 2

[21] ANSI/ASHRAE/IES Standard 90.1-2010 (I-P), 2010. 2

[22] CSTB. Methode de calcul ThB-CE. Technical report, 2013. 2

[23] Ken Bruton, Paul Raftery, Barry Kennedy, Marcus M. Keane, and D. T. J. O'Sullivan. Review of automated fault detection and diagnostic tools in air handling units. *Energy Efficiency*, 7(2):335–351, April 2014. 2

[24] Yuebin Yu, Denchai Woradechjumroen, and Daihong Yu. A review of fault detection and diagnosis methodologies on air-handling units. *Energy and Buildings*, 82:550–562, October 2014.

[25] Haitao Wang, Youming Chen, Cary W.H. Chan, and Jianying Qin. A robust fault detection and diagnosis strategy for pressure-independent VAV terminals of real office buildings. *Energy and Buildings*, 43(7):1774–1783, July 2011.

[26] Haitao Wang, Youming Chen, Cary W.H. Chan, Jianying Qin, and Jinhua Wang. Online model-based fault detection and diagnosis strategy for VAV air handling units. *Energy and Buildings*, 55:252–263, December 2012.

[27] Haitao Wang and Youming Chen. A robust fault detection and diagnosis strategy for multiple faults of VAV air handling units. *Energy and Buildings*, 127:442–451, September 2016. 2

[28] Alessandro Beghi, Luca Cecchinato, Fabio Paggiaro, and Mirco Rampazzo. VAVAC Systems Modeling and Simulation for FDD Applications. page 6, 2011. 2

[29] Rongpeng Zhang and Tianzhen Hong. Modeling of HVAC operational faults in building performance simulation. *Applied Energy*, 202:178–188, September 2017. 2

[30] JO (1983). Arrêté du 24 mars 1982 relatif à l'aération des logements, March 1982. 2, 3

[31] JO(1984). RSDT - Règlementation Sanitaire Départemental Type, May 1984. 3

[32] Janghyun Kim, Stephen Frank, James E. Braun, and David Goldwasser. Representing Small Commercial Building Faults in EnergyPlus, Part I: Model Development. *Buildings*, 9(11):233, November 2019. 5

[33] Ando Andriamamonjy, Dirk Saelens, and Ralf Klein. An auto-deployed model-based fault detection and diagnosis approach for air handling units using bim and modelica. *Automation in Construction*, 96:508–526, 2018.

[34] Raymond Sterling, Gregory Provan, Jesús Febres, Dominic O'Sullivan, Peter Struss, and Marcus M. Keane. Model-based Fault Detection and Diagnosis of Air Handling Units: A Comparison of Methodologies. *Energy Procedia*, 62:686–693, 2014.

[35] Shokouh Pourarian, Jin Wen, Xiwang Li, Daniel Veronica, Xiaohui Zhou, and Ran Liu. Tools for evaluating air flow network of dual duct double fan systems. *ASHRAE/IBPSA-USA Bldg Simulation Conf, Atlanta, GA*, pages 1–9, 2014.

[36] Steven T Bushby, Natascha Castro, Michael A Galler, and Cheol Park. Using the virtual cybernetic building testbed and FDD test shell for FDD tool development. Technical Report NIST IR 6818, National Institute of Standards and Technology, Gaithersburg, MD, 2001. 5

[37] ASHRAE. Method of Testing Air-to-Air Heat/Energy Exchangers - ANSI/ASHRAE Standard 84-2013, 2013. 7

[38] Air conditionning, Heating & Refregiration Institute. AHRI Standard 1061 (SI) - 2018 Standard for Performance Rating of Air-to-Air Exchangers for Energy Recovery Ventilation Equipement.pdf, 2018. 7

[39] ASHRAE Guideline 2 (RA96). Engineering Analysis of Experimental Data issn 1049-894x, 1986. 7

[40] John R. Taylor. *An Introduction to Error Analysis: The Study of Uncertainties in Physical Measurements*. University Science Books, Sausalito, California, 1997. 7

[41] T. Agami Reddy. *Making Statistical Inferences from Samples*, pages 103–140. Springer US, Boston, MA, 2011. 7

[42] P. Haves. Fault modelling in component-based HVAC simulation. In *Proceedings of Building Simulation 1997*, Prague , Czech Republic, 1997. 9

[43] Shengwei Wang, Qiang Zhou, and Fu Xiao. A system-level fault detection and diagnosis strategy for HVAC systems involving sensor faults. *Energy and Buildings*, 42(4):477–490, April 2010. 9

[44] Sanja Lazarova-Molnar, Hamid Reza Shaker, Nader Mohamed, and Bo Norregaard Jorgensen. Fault detection and diagnosis for smart buildings: State of the art, trends and challenges. In *2016 3rd MEC International Conference on Big Data and Smart City (ICBDSC)*, pages 1–7, Muscat, March 2016. IEEE. 9

[45] R. Yan, Z. Ma, G. Kokogiannakis, and Y. Zhao. A sensor fault detection strategy for air handling units using cluster analysis. *Automation in Construction*, 70:77–88, 2016. 9

[46] H. Geoffroy, J. Berger, B. Colange, S. Lespinats, D. Dutykh, C. Buhe, and G. Sauce. Use Of Multidimensional Scaling For Fault Detection Or Monitoring Support In A Continuous Commissioning. pages 877–884, Rome, Italy, 2019. 25

[47] Hugo Geffroy, Julien Berger, Benoit Colange, , Sylvain Lespinats, and Denys Dutykh. The use of dimensionality reduction techniques for fault detection and diagnosis in a ahu unit: critical assessment of its reliability. *under submission*, pages 1–26, 2021. 25